Macromolecules
ARTICLE

Macromolecules **2009**, *42*, 6761–6776 **6761**
DOI: 10.1021/ma9008324

Theory of Cluster Formation in Homopolymer Melts

A. N. Semenov*

Institut Charles Sadron, CNRS - UPR 22, 23 rue du Loess, BP 84047, 67034 Strasbourg Cedex 2, France

Received April 16, 2009; Revised Manuscript Received July 14, 2009

ABSTRACT: A physical mechanism of micelle formation in homopolymer systems is elucidated. The mechanism is applicable in particular to melts of stereoisomeric polymers, for example, polystyrene. It is hinged on aggregation and crystallization of occasional atypical stereoregular fragments of mostly irregular (atactic) polymer chains. Phase diagrams involving the regimes of lamellar, tapelike, and disklike semicrystalline micelles are obtained and discussed. The possible relevance of the theory to the puzzling anomalous cluster phenomena observed in homopolymer melts (low-frequency solidlike rheological behavior; low-q excess light scattering−Fischer cluster modes) is discussed as well.

1. Introduction

Aggregation phenomena are common in polymer systems.[1,2] One can roughly distinguish between two types of aggregates: (1) those that grow indefinitely and (2) stable finite clusters (multimers). Aggregation of the first type can be due to a phase separation related to a macroscopic phase transition like liquid−liquid separation in a two-component system (polymer + poor solvent, or a mixture of two polymers). On the other hand, multimerization, i.e., formation of stable finite aggregates (micelles), is typical for amphiphilic polymers containing (at least) two types of chemical units in polymer chain. The well-known examples of such systems are block copolymers in selective solvents, associating polymers, polysoaps, hydrophobic polyelectrolytes, biopolymers, etc.[3]

Micelles stabilized by amphiphilicity are relatively well understood theoretically.[1,3,2,4−8] Compact finite aggregates can be also stabilized by other factors, notably, by electrostatic effects or by chirality-induced frustrations.[9] In all the cases micelle formation requires at least two components, for example, solvent and structure-forming polymer.[10]

There are, however, many indications that some thermodynamically stable aggregates (clusters) are formed in homopolymer melts (single-component systems) in conditions far away from any known phase separation. In particular, static and dynamic light-scattering studies routinely reveal the presence of an anomalous *cluster mode* in different homopolymer systems (polymer melts, polymers dissolved in good solvents, compatible binary homopolymer mixtures).[11−16] The mode is characterized by anomalously high scattering intensity and slow relaxation rate at low wave-vector q. It is often referred to as "Fischer cluster mode" marking the outstanding contribution of E. W. Fischer and his colleagues to the detailed investigations of such anomalous scattering.[11−13] The Fischer mode can be interpreted as being due to the presence of a small amount of large clusters with typical size 100−300 nm (much larger than the polymer chain gyration radius). The cluster mode was also observed in block copolymers.[17−19]

Another bulk of evidence on clusters comes from rheological experiments:[20−23,25,27] it was recently found that many homopolymer melts show solidlike behavior at low frequencies in micrometer-thick layers. These puzzling results (which were strongly challenged for possible artifacts, no definitive source of error being identified[21−26]) are pointing to formation of some long-range clusters[20] that are possibly bridging across the layer.

These cluster phenomena (low-q scattering, low-frequency elasticity) are hardly explicable by any of the known theoretical mechanisms:

(i) A phase separation can give rise to a transient heterogeneous structure of, say, mesoscopic domains of one phase in the matrix of the other phase. Can such domains play a role of "clusters"? There are two problems with this picture: First, according to the Gibbs phase rule, phase equilibrium in a pure one-component system is only possible at a fixed temperature T, while the cluster-related phenomena are observed in a wide T-range. Second, it concerns nonequilibrium transient conditions where the domain size must continuously increase in time. Experimentally, the correlation length and other parameters of the cluster mode do not change after some equilibration time.[11,12]

(ii) One can argue that even a homopolymer melt is formally not a single-component system due to polydispersity. However, it is clear that polydispersity itself cannot lead to a phase separation (at least to my knowledge, a polydispersity-induced phase segregation in homopolymers was never observed or predicted). Besides, similar "cluster phenomena" were observed in polymer systems with various degrees of polydispersity ($M_w/M_n - 1 = 0.09-0.9$[12−14]).

(iii) Several authors proposed the idea of fluidlike and solidlike correlated regions in glass-forming liquids.[11,28−31] This qualitative idea, however, is not supported by a consistent quantitative theory. The proposed picture of correlated domains seems to be applicable only close to the glass transition T_g (whereas "cluster" phenomena are observed 100 °C above T_g). In addition, the size of the "correlated regions" is expected to be of the order of a few nanometers (it corresponds to the size of cooperative regions associated with α-relaxation[13] or to the Boson peak[31]); i.e., it is much smaller than the apparent cluster size (typically ∼100 nm).

(iv) The low-q cluster mode scattering intensity is in contradiction with the thermodynamic rule relating

Published on Web 08/14/2009

it with the isothermal compressibility of the system:[11] the experimental low-q structure factor $S(q)|_{q\to 0}$ is much higher than that prescribed by the fluctuation−dissipation theorem, i.e., than

$$S(q)\Big|_{q\to 0} = S_T \equiv k_B T \rho \frac{\partial \rho}{\partial p}\Big|_{T=\text{const}} \quad (1)$$

where the theoretical S_T is proportional to the isothermal compressibility $(1/\rho)(\partial\rho/\partial p)|_{T=\text{const}}$. Trying to rationalize this contradiction, E. W. Fischer resorted to nonequilibrium and nonergodic effects arguing that they can be related to the glass transition. While nonequilibrium effects are always an issue in polymer systems, the relevance of the glass transition for the "cluster mode" observed well above T_g must be questioned. In addition, it seems that completely ergodic behavior is re-established at time scales longer than the relaxation time of the cluster mode,[11] while the thermodynamic relationship is strongly violated even at the longest time scales.

Thus, even the driving force for the cluster formation is of unclear origin (not to say about the factors controlling their finite apparently equilibrium size).

In the present paper we consider a new mechanism of cluster formation in homopolymers that may be relevant to the experimental results mentioned above. The theory is applicable to stereoisomeric homopolymers. It shows that even incompressible homopolymer melts at complete equilibrium can exhibit strong low-q excess scattering. The main idea concerning the origin of clusters in homopolymers is described in the next section. The physical model and the free energy of homopolymer aggregates (semicrystalline micelles) are considered in section 3. The main results are presented in section 4, where the micelle formation in polystyrene melts is considered as the primary example; the results are discussed in the last section.

2. Clusters in Atactic Homopolymers: The Central Idea

2.1. Stereoisomerism and Tacticity. Many homopolymers are stereoisomeric. This means that their repeat units involve chemical bonds whose mutual orientations can be chosen in a number of different ways, while the orientational choice is virtually permanent: it cannot be changed dynamically during the system lifetime. The most common types of such geometrical isomerism are tacticity and cis−trans isomerism.

Many vinyl and other polymers are characterized by tacticity. The simplest example is polystyrene (PS). Each of its aromatic side groups can be positioned either to the left (L) or to the right (D) of the main chain (it is assumed that the backbone orientation and direction are specified; note that each PS unit has an asymmetric center and becomes formally chiral once a direction along the backbone is specified, so the D and L units can be formally considered as enantiomers).

Thus, the stereoisomeric state of a PS chain can be defined as a sequence of side group orientations (DLLD...). One can distinguish the following important cases (Figure 1a−c): *isotactic* polymer (iPS) with the same orientation of all side groups (e.g., DDDDDD...), *syndiotactic* polymer (sPS) with regular alternating orientations of side groups (DLDLDL...), and *atactic* isomers characterized by a random sequence of side orientations (like DDDLLD...). The ordinary commercial PS is atactic. Isotactic and syndiotactic chains can be synthesized using an appropriate catalyst (Ziegler−Natta catalysis[33] or metallocene catalysis[34]).

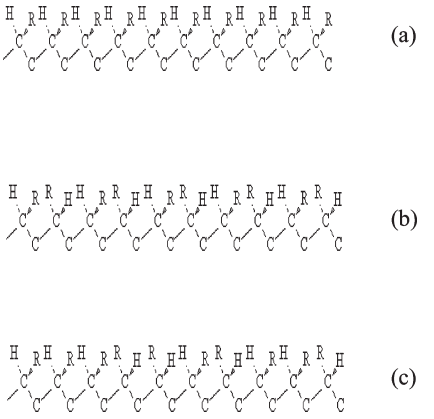

Figure 1. Different geometrical isomers of polystyrene (PS); R stands for aromatic ring: (a) isotactic polymer, iPS; (b) syndiotactic polymer, sPS; (c) atactic polymer, aPS.

A stereoisomeric polymer can be characterized by the fraction f_m of *meso* diads (DD or LL); the fraction of *racemo* diads (DL or LD) is $f_r = 1 - f_m$. The meso and racemo states are physically different, so generally $f_m \neq f_r$. The racemo state is often more favorable due to higher rotational freedom of side groups in this state as compared with meso state. $f_m = 1$ for ideal isotactic polymer, and $f_m = 0$ for syndiotactic polymer. In the general atactic case $f_m/f_r = e^{\Delta\varepsilon}$, so that $f_m = 1/(1 + e^{-\Delta\varepsilon})$. The parameter $|\Delta\varepsilon|$ can serve as a measure of the degree of tacticity of atactic polymer. More precisely, the degree of tacticity can be defined as $d_t \equiv |f_m - f_r| = \tanh(|\Delta\varepsilon|/2)$; it changes from 0 for completely random sequence of isomers to 1 for perfectly isotactic or syndiotactic sequences.

If the isomeric state is defined by equilibrium factors, then $\Delta\varepsilon$ can be interpreted as the free energy difference between meso and racemo diads, divided by $k_B T$, at the conditions where the polymer stereochemical configuration was defined. Typically $|\Delta\varepsilon| \lesssim 1$ for vinyl polymers. In particular, $f_m = 0.3-0.5$ for conventional atactic polystyrenes[36−38] corresponding to $|\Delta\varepsilon| = 0-0.85$.

There are chemical procedures allowing transformations between L and D isomers (epimerization[35]). At the stereochemical equilibrium (that can be established as a result) both f_m and $\Delta\varepsilon$ are T-dependent. For PS it was found[35]

$$f_m = \frac{2(1+\eta)}{(2+\eta)^2}, \quad \eta \approx 0.5 \exp(350/T)$$

where T is the absolute temperature, leading to $f_m \approx 0.4$ at room T. In the general case, polymers with arbitrary degree of tacticity can be obtained by epimerization of initially isotactic or syndiotactic polymers.[35]

Interactions between non-nearest-neighboring side groups can normally be neglected. Hence, the macromolecular stereoisomeric sequence can be considered as a Markovian (Bernoullian) process, so that the whole sequence statistics is defined by f_m. For example, the probability of an isotactic triad (LLL or DDD) is f_m^2.

Physical properties of isomeric homopolymers strongly depend on their stereochemical structure. Irregular (atactic) polymers are normally glass-formers. Stereoregular (e.g., isotactic or syndiotactic) polymers typically crystallize. The glass transition temperature T_g of atactic PS (aPS) of molecular weight $M > 4000$ is in the range 70−100 °C; it can be approximated as

$$T_g \approx 100 - 1200/N \ (^\circ\text{C}) \quad (2)$$

where N is the polymerization degree.[41,40,39] Stereoregular PS (iPS, sPS) crystallize below $T_m \approx 240-270$ °C.

2.2. Physical Nature of Aggregation in Stereoisomeric Polymers. Most homopolymers exhibiting anomalous phenomena associated with clusters are stereoisomeric (atactic). Such stereoirregular homopolymers must be considered as intrinsically multicomponent systems: each specific sequence (DLLLDD...) is a component. Therefore, the thermodynamic rule, eq 1, is not applicable to these homopolymers since this rule is established for pure single-component systems. The natural questions are: What could be the implications of irregular stereoisomeric polymer chain structure for physical properties of polymer melts? In particular, can the isomeric structure be responsible for cluster formation?

Trying to clarify these points, we first note that the sequence diversity of atactic polymers is similar to that of random copolymers consisting of two types of monomer units (say, A and B). Undiluted molten random copolymers show interesting structural properties including formation of multiplets and clusters (ionomers, associating polymers),[42−44,76,75] microdomain structures with various domain geometries and length scales,[45−49] hierarchical structures,[50−53] and micelles with internal or surface patterns.[54,55] The predicted heterogeneities in random copolymers are also responsible for their unusual dynamical properties.[57,75]

Can we anticipate that atactic homopolymers tend to form domains or clusters which are similar in nature to heterogeneities in random copolymers?

The answer is not exactly positive: All sorts of structures formed in AB copolymers are driven by the thermodynamic incompatibility between A and B units, which is described by positive Flory interaction parameter ($\chi_{AB} > 0$): the AAA... and BBB... blocks tend to segregate as a result. This effect is absent in atactic homopolymers (like PS) since DDD... and LLL... blocks are physically equivalent and the corresponding interaction parameter $\chi_{LD} = 0$.

Nevertheless, a tendency for domain (micelle) formation does exist in atactic polymers. The main notion is that their globally random chain sequences occasionally include stereoregular (isotactic or syndiotactic) fragments of, say, n consecutive units (Figure 2). Although the fraction ϕ of such fragments is low, it is not negligible unless n is very high. For example, for a completely random DL sequence the fraction of isotactic fragments of length 10 (or longer) is around 1%. It is also important that the glass transition temperature T_g of an atactic homopolymer is normally significantly lower than the crystallization temperature T_m of its stereoregular isomer. For example, in the case of PS there is a wide window (of width $T_m - T_g \gtrsim 150$ °C) above T_g where (i) the atactic polymer is basically liquidlike and (ii) the stereoregular chain fragments can form crystals.

The most common (and the simplest) polymer crystal structure is lamellar;[100,101] it corresponds to relatively thick sheets in which polymer stems are arranged in a regular way; the stem chain axis is aligned essentially perpendicular to the sheet (along its thin direction). Typically, the sheet thickness (= the stem length) is ~10 nm, while the lateral sheet extension is much longer (it can be ~ 10 μm or greater).

The following process can be therefore anticipated in a temperature range, $T_g < T < T_m$: first, the atypical stereoregular fragments aggregate; second, they adopt an extended (helical or zigzag) conformation and crystallize forming a lamellar crystal. The crystallized stereoregular fragments are surrounded by amorphous atactic *tails* forming a corona. Micelles with core/shell structure are formed as a result. Examples of such core/shell lamellar aggregates are shown in Figure 3. Note that the volume fraction of the micelles is expected to be small, comparable with $\phi \lesssim 1\%$. The micelles can be thermodynamically stable since the free energy gain on crystallization (which is proportional to n per chain) may overwhelm the entropic penalty implied by aggregation. This idea is backed by a quantitative theory presented in the next section. We argue below (see the discussion in section 5) that such semicrystalline aggregates (micelles) can give rise to the anomalous cluster-related phenomena (low-q scattering, low-frequency elasticity) mentioned in the Introduction.

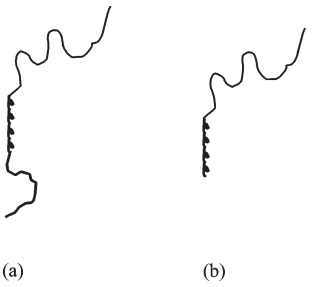

Figure 2. Polymer chain with stereoregular fragment (shown as a thick line) in the middle (a) and at the end (b). Note that atactic tails (thinner lines) may be actually considerably longer than the stereoregular part.

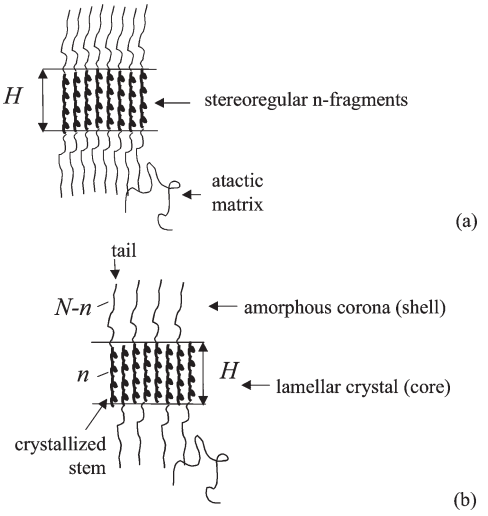

Figure 3. Semicrystalline core/shell lamellar micelles formed by polymer chains shown in Figure 2a,b. The core of thickness H is a lamellar crystal formed by stereoregular fragments (stems of n units each). The amorphous corona (shell) is formed by atactic chain tails. A tail consists of $N - n$ units in the structure (b) where stereoregular fragments are located near the chain ends.

3. Semicrystalline Micelles in Homopolymer Melts: The Physical Model and the Free Energy

3.1. Free Energy of Lamellar Micelles. *3.1.1. Lamellar Structure*. We now turn to a more quantitative description of clustering in stereoisomeric homopolymers. We first consider lamellar micelles with crystalline core and amorphous shell (see Figure 3). The crystalline layer consists of stereoregular stems of n units; the layer thickness is $H = L_1 n$, where L_1 is the stem length per chemical unit (thus H is the end-to-end length of a crystallized chain fragment which adopts a regular conformation, typically either helical, like in iPS, or a planar zigzag, like in sPS). Stereoregular fragments appear by chance; hence, they can be located anywhere on polymer chain. It is therefore tempting to assume that each chain involved in the lamellar aggregate contains a crystallized stereoregular n-fragment and two tails, N_1 and N_2; the tails

are long: the mean tail length is $0.5(N-n) \gg 1$, where N is the overall number of units in a chain (see Figures 3a and 2a). This picture however is not realistic. The reason is simple: The crystal density in normally significantly higher than the density of amorphous polymer (for example, the density of atactic amorphous PS is $\rho_m \approx 0.95$ g/cm^3, while $\rho_c \approx 1.05$ g/cm^3 in crystallized iPS or sPS). Simultaneously, the chains are locally stretched almost to the maximum degree in the crystal structure. This means that even if free polymer chains (those not connected to the micelle) do not penetrate in the micellar shell, the chain tails in the shell have to be overstretched (by ~10% beyond the maximum elongation), leading to a high free energy penalty. We therefore have to adopt an alternative picture (Figures 2b and 3b) where one of tails is very short or absent.[85]

3.1.2. Fraction of Micelles. Let us estimate the volume fraction ϕ occupied by the micelles (clusters) with crystal core of thickness $H = nL_1$. For simplicity, we consider aggregation of isotactic fragments ($\Delta\varepsilon > 0$) located exactly at a chain end (i.e., the second atactic tail is not allowed; lifting this approximation leads to a somewhat higher stability of micelles and a higher ϕ). Then ϕ is just the probability that a chain has such end-fragment of length n or longer (it is these chains that aggregate and form micelles):

$$\phi \simeq 2f_m^{n-1} = \frac{2}{(1+e^{-\Delta\varepsilon})^{n-1}} \tag{3}$$

where the factor 2 accounts for two chain ends, and it is assumed that $N - n \gg 1$. If syndiotactic subsequences are favored (i.e., if $\Delta\varepsilon < 0$), then ϕ is still defined by eq 3 provided that $\Delta\varepsilon$ is replaced by $|\Delta\varepsilon|$. Typically, for large n, $\phi \ll 1$: only a small fraction of chains contain long enough stereoregular fragments.

3.1.3. Free Energy. The excess micelle free energy, i.e., the free energy change (per chain) on micelle formation from a disordered melt, can be represented as a sum of several terms:

$$F_{lam} \simeq \Delta F_{cryst} + F_{entr} + F_{face} + F_{conf} \tag{4}$$

Here the disordered melt is considered as a reference state, $F_{dis} = 0$, and F_{lam} is the free energy per aggregating chain. The four terms in the right-hand side of eq 4 represent the (negative) free energy due to crystallization of micelle core, the free energy increase related to the translational entropy of aggregating chains, the crystal (core) interfacial energy, and the conformational free energy of amorphous tails in the shell.

ΔF_{cryst}, the extensive free energy gain on crystallization, is

$$\Delta F_{cryst} \simeq -k_B S_m n (T_m - T) \tag{5}$$

where k_B is the Boltzmann constant, T_m is the ideal crystallization temperature, T is the current absolute temperature, and $S_m = M_1 H_m/(R_{gas} T_m)$ is the corresponding entropy of melting per unit (for 100% crystallized infinitely long chains). Higher-order terms in $T_m - T$ are omitted in eq 5. Here M_1 is the mass of chemical unit, $R_{gas} = k_B N_A$ is the universal gas constant, and H_m is the enthalpy of melting per unit mass. Thus

$$\frac{\Delta F_{cryst}}{k_B T} \simeq -S_m n \tau, \quad \tau \equiv \frac{T_m}{T} - 1 \tag{6}$$

where τ is the temperature parameter.[86]

The second term in eq 4 accounts for the entropy loss due to a low fraction of stereoregular chain fragments. In disordered state the ends of stereoregular fragments are uniformly distributed in space, whereas upon micelle formation these ends have to be located in thin sublayers at the surface of lamellar crystals. The available volume thus reduces from V_{tot} to $\simeq (2/N)\phi V_{tot}$; therefore

$$\frac{F_{entr}}{k_B T} \simeq -\ln\left(\frac{2}{N}\phi\right) = \ln(N/4) + (n-1)\beta,$$
$$\beta \equiv \ln(1 + e^{-|\Delta\varepsilon|}) \tag{7}$$

where the first factor $(2/N)$ is the fraction of volume available for chain ends inside a core/shell lamellar aggregate ($2L_1$ is the thickness of two surface sublayers, NL_1 is roughly the total thickness of the core/shell lamella) and ϕ is the volume fraction of all lamellae. The parameter β depends on the degree of tacticity, changing from $\beta = \ln 2$ for completely random sequence to a small $\beta \simeq e^{-\Delta\varepsilon} \simeq f_r$ for $\Delta\varepsilon \gg 1$.

The next term is the core/shell interfacial energy: $F_{face} = 2A_1\gamma$, where γ is the face surface tension of crystal lamella and A_1 is the area per chain in the crystalline core ($A_1 = M_1/N_A L_1 \rho_c$, where ρ_c is the core density). Thus

$$\frac{F_{face}}{k_B T} = 2J = 2J_0(1+\tau) \tag{8}$$

where $J \equiv A_1\gamma/(k_B T)$. Generally γ depends on T; for simplicity, this dependence is ignored here: $\gamma = \text{const}$, $J = J_0(1+\tau)$, where $J_0 = J|_{T=T_m}$.

The last term F_{conf} is the conformational free energy due to elongation of tails in the shell (corona). The shell can be considered as a rather dense polymer brush at each side of the crystalline core. Applying the standard theory of end-grafted polymer brush,[58−60] we get

$$\frac{F_{conf}}{k_B T} \simeq \frac{3}{2}\frac{\tilde{H}^2}{\tilde{N}b^2} = \frac{3}{2}\frac{\tilde{L}_1^{\,2}}{b^2}\tilde{N} \tag{9}$$

where $\tilde{N} = N - n$ is the number of units in a tail, $\tilde{H} = \tilde{L}_1 \tilde{N}$ is the thickness of one brush ($2\tilde{H} + H$ is thus the total thickness of lamellar micelle), b is the statistical segment of amorphous polymer

$$\tilde{L}_1 = \frac{\rho_c}{2\rho_m} L_1 \tag{10}$$

is the mean projection of a tail unit onto the normal to the layer, and ρ_m is the density in the shell which is assumed to be close to that in the amorphous melt.

Here we assumed for simplicity that polymer chains are monodisperse and used the Alexander−de Gennes approximation.[58−60] This approximation overestimates the brush elastic energy by about 22%.[61,62] It is used for consistency with the treatment of nonlamellar morphologies (see section 3.3) where analytical implementation of the more precise approach[61,62] appears to be too complicated.

Further, we considered the tails as Gaussian chains (neglected their limited extensibility) and neglected an interpenetration between the brush and the surrounding free chains. The last effect gives rise to a small decrement of the brush energy[63,64] (the relative correction is $\sim(g/\tilde{N})^{1/3}$, where g is the elastic blob size defined by the grafting density).

We also neglected the direct effect of solid crystal surface to which the tails are attached on their configurational entropy. In the regime of no solvent (molten amorphous corona) the free energy penalty due to the solid surface effect

(a reduction of the configurational space available to the tails due to the impenetrable surface) is totally equivalent to a renormalization of the face surface energy (the tension γ). The reason is that the effect can be reduced to local monomer/surface interactions and to local perturbations of amorphous chain conformations (affecting the short chain fragments—blobs—near the surface). There are other more subtle corrections on the top of this crude effect in the brush regime. A concise analysis of the additional surface effect (related to the so-called proximal layer) can be found in ref 64. For the standard model (incompressible melt, Gaussian chains) the latter effect results in a free energy correction (per chain in k_BT energy units) $\Delta F = -\ln 2 + \Delta F_\mu$, where $-\ln 2$ comes from the reflection principle,[98,99] and ΔF_μ is the proximal layer correction,[64] $\Delta F_\mu \approx 0.19$ for the Alexander–de Gennes brush (the correction is a bit lower for a parabolic brush[64]). In any case, the ΔF correction is small (as compared with other free energy terms), and moreover, in the brush regime with constant grafting density it can be considered merely as a moderate contribution to the crystal face tension γ.

As for the Gaussian elasticity approximation, it can be assessed resorting to a more realistic model treating a polymer tail as a long freely jointed chain of rods[65] that does show a limited extensibility: The essential parameter is the degree of elongation η (the ratio of the end-to-end distance to the contour length of the chain). For finite η the elastic energy F_{el} is proportional to the following function of the reduced force f: $F_{el} = \text{const}\,(f\eta - \ln[\sinh(f)/f])$ where $\eta = (1/\tanh f) - 1/f$; the elastic energy of the corresponding Gaussian chain is $F_{el}^{(G)} = \text{const}\ {}^3/_2\eta^2$, with the same constant. The ratio $r = F_{el}/F_{el}^{(G)}$ is thus a function of η. The degree of elongation in the shell of atactic tails is (see eq 10)

$$\eta \approx \frac{\tilde{L}_1}{L_1} \approx 0.5$$

The factor r corresponding to this η is $r \approx 1.1$, meaning that the Gaussian chain approximation underestimates the elastic energy by ~10%. Note that the two approximations (Alexander–de Gennes and Gaussian elasticity) bring in corrections that partially compensate each other, so the overall accuracy of the simple eq 9 is roughly 10%.

3.2. Disordered Melt→Lamellar Micelle Transition. *3.2.1. Limiting Temperature.* The thermodynamic transition (formation of lamellar aggregates) occurs at $F_{lam} = F_{dis} = 0$; F_{lam} is defined by eqs 4–9. The transition temperature T_{dl} depends on n, $\Delta\varepsilon$, and other parameters. In particular, T_{dl} increases with the lamellar thickness n. For $n \to \infty$ (more precisely, for $N = n \to \infty$) the equation $F_{lam} = 0$ simplifies as $-S_m\tau + \beta = 0$ defining the limiting transition temperature

$$T^* = \frac{T_m}{1 + \beta/S_m} \tag{11}$$

where $\beta \equiv \ln(1 + e^{-|\Delta\varepsilon|})$. Obviously, T^* increases with $|\Delta\varepsilon|$ and approaches T_m at large $|\Delta\varepsilon|$.

3.2.2. Relevance of Polystyrene. To further illustrate this result, let us consider aggregation in a melt of aPS. Polystyrene is chosen since it is one of the simplest stereoisomeric polymers which shows anomalous phenomena (low-frequency elasticity); another reason is that the relevant physical properties of PS are known better than for most other polymers. As mentioned above, $f_m < 0.5$ and $\Delta\varepsilon < 0$ for conventional aPS, meaning a preference for formation of syndiotactic subsequences (rather than isotactic). It is important, however, that crystallization of syndiotactic PS, sPS, is less studied in comparison with isotactic PS, iPS (sPS was synthesized rather recently[66,67]), so the relevant for the theory crystallization parameters of sPS are either not known or known with lower confidence than for iPS. For these reasons, it is clusters involving isotactic crystals of PS that are considered in the present paper for illustrative purposes. Accordingly, the sign of $\Delta\varepsilon$ is simply inverted; i.e., the regime $\Delta\varepsilon > 0$ is considered to ensure formation of micelles with isotactic cores. This is reasonable, since the combinatorial entropic penalty for isotactic fragments depends on the magnitude $|\Delta\varepsilon|$ (defining the degree of tacticity), so the sign inversion does not change it. As for the magnitude $|\Delta\varepsilon|$, we consider the typical regime, $|\Delta\varepsilon| \lesssim 1$, as discussed in section 2.1. Note that crystallization temperature T_m is higher for sPS than for iPS, so an even wider "cluster T-window" may be expected for sPS.

3.2.3. Crystallization Parameters for PS: T_m, S_m, J. In order to proceed, we have to know T_m, H_m, and other parameters characterizing iPS crystallization. The commonly reported crystallization parameters for iPS are $T_m^{(a)} \approx 240$ °C and $H_m^{(a)} \approx 87$ J/g.[68] Here the superscript "(a)" signifies "apparent" values based on the data on typical semicrystalline iPS.

The apparent parameters include, in particular, the effect of interfaces between crystalline and amorphous regions. In order to get "ideal" parameters (T_m, H_m) required for the theory, one has to perform extrapolation to the infinite thickness H of crystal layers and to the infinite molecular weight M. A detailed analysis of the H-dependence of the melting temperature for iPS was performed by Strobl et al.[69,70] The extrapolated equilibrium parameters are

$$T_m \approx 266\ ^\circ\text{C}, \quad H_m \approx 89.5\text{J/g}\ (\approx 9.3\ \text{kJ/mol}) \tag{12}$$

(Note that the extrapolation procedure is not very precise; in fact, an even higher $T_m \approx 289$ °C was obtained in the earlier study.[69]) Assuming that the apparent melting temperature $T_m^{(a)}$ for a given H is defined thermodynamically, we get the condition

$$-k_BS_m(T_m - T_m^{(a)}) + 2\gamma A_1\frac{L_1}{H} = 0 \tag{13}$$

hence

$$T_m^{(a)} = T_m - \frac{2\gamma A_1 L_1}{k_B S_m}\frac{1}{H} \tag{14}$$

The crystal face tension γ (and the reduced tension J_0) can be then calculated based on the experimental dependence of $T_m^{(a)}$ vs $1/H$ using the parameters, eq 12. Thus we get

$$S_m \approx 2.1, \quad J_0 \approx 1.95 \tag{15}$$

Note that the parameter J (or J_0) estimated based on the data on crystallization of isotactic PS melts is probably overestimated: The crystal face structure there involves a lot of short amorphous loops that increase the face energy. Such loops are characteristic of standard crystallization of stereoregular polymers, but they are absent in the case of lamellar crystal formation by atactic polymers (see Figure 3b), leading to a lower effective J in the latter case. In turn, a lower J leads to a *wider* region of stability of semicrystalline micelles for atactic polymers.

The $M \to \infty$ extrapolation was not done in refs 69 and 70 as the experimental data were obtained for the molecular weight $M \approx 4 \times 10^5$.[71] This M is rather high (the chains

are more than 100 times longer than crystal stems), so the finite-M effects are perhaps weak.

There are, however, more significant effects that could lead to higher effective values of the parameters T_m and S_m even with respect to the experimental values that were perfectly extrapolated for $H \to \infty$ and $M \to \infty$. The reasons are twofold.

(i) On the one hand, iPS is a semicrystalline polymer with typical degree of crystallinity of 30−40%.[72] The semicrystalline structure implies that the amorphous layers are (at least partially) "trapped" between crystals, so the amorphous regions can hardly be relaxed due to geometrical and topological restrictions imposed by the neighboring crystals. (In fact, an amorphous layer is partially formed by polymer chains that also enter in the crystals.) The semicrystalline state is therefore somewhat destabilized (has higher free energy) even in the limit $H \to \infty$ in comparison with an ideal equilibrium crystal structure. As a result, the T_m and S_m obtained from the iPS crystallization data must be underestimated.

(ii) Another source of error comes from the difference between a crystallization/melting of a neat iPS (whose studies serve to yield the thermodynamic parameters in question) and crystallization of occasional isotactic fragments in the atactic matrix (as considered in the present paper). In the latter case, there is always an incompatibility between isotactic and atactic components (an excess enthalpy of their mixing) that provides an additional driving force for aggregation of stereoregular fragments (for micelle core crystal formation). This effect leads to larger free energy difference between the disordered and the aggregated states (in favor of micelles), i.e., again to larger effective values of T_m.

To resume, both effects considered above must enlarge the region of micelle (cluster) stability. However, as there seem to be no means at present to estimate these effects quantitatively, we have to ignore them in what follows (although they may lead to, say, a significant increase of T_m).

3.2.4. Transition Temperatures for aPS. The dependence of T^* on the degree of tacticity $d_t \equiv |f_m - f_r| = \tanh(|\Delta\varepsilon|/2)$ obtained using the estimated parameters T_m and S_m for aPS, eq 15, is plotted in Figure 4 in the relevant range $|\Delta\varepsilon| \lesssim 1$. T^* changes from ≈130 to ≈200 °C (for comparison, a low-frequency elasticity of PS melts has been revealed[20] at T's up to ≈ 140 °C).

The transition temperature T_{dl} depends on the lamellar thickness (n), the degree of tacticity (d_t), and polymer molecular weight (N). T_{dl} for PS (in °C) is plotted vs N in Figure 5 for two values of d_t (1/5 and 1/3, corresponding to $\Delta\varepsilon \approx 0.405$ and 0.69, respectively) and for two lamellar thicknesses: the "maximum" thickness ($n = N$) and the thickness $n = n(\phi)$ corresponding to a certain volume fraction of micelles, $\phi = 10^{-4}$ (the dependence $n(\phi)$ is implicitly defined in eq 3). It is obvious that lamellar micelles with $\phi = 10^{-4}$ are stable above the glass transition temperature T_g if N is not too high ($N < 80$ for $d_t = 1/5$ and $N < 160$ for $d_t = 1/3$).

3.3. Nonlamellar Morphologies. As shown above, the lamellar micelles are getting destabilized as the chain length N increases: the elastic energy of the corona, which is roughly proportional to N, works against the lamellar micelle formation. This does not mean however that micelle formation is not possible for very high N: rather, in this regime

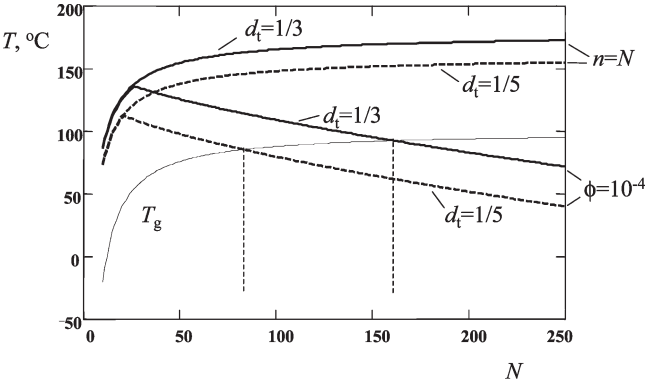

Figure 5. Dependence of the dis → lam transition temperature T_{dl} on the polymerization degree N for aPS. The upper pair of curves correspond to $n = N$, and the lower pair of curves correspond to the volume fraction of micelles $\phi = 10^{-4}$; solid lines correspond to $d_t = 1/3$; dashed lines, $d_t = 1/5$. The glass transition temperature T_g, eq 2, is shown as well. The vertical dashed lines mark the highest N allowing for formation of lamellar micelles above T_g.

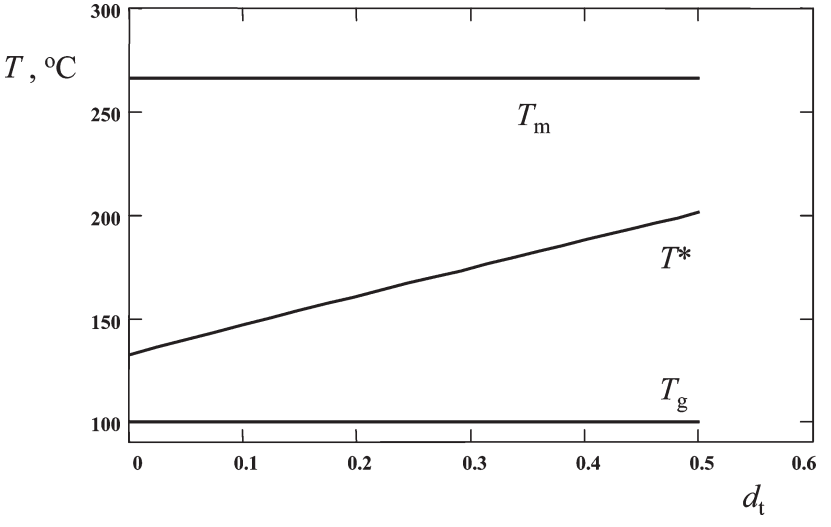

Figure 4. Dependence of the limiting dis → lam transition temperature T for $N = n \to \infty$ on the degree of tacticity d_t for aPS. The crystallization (T_m) and glass transition (T_g) temperatures for $N \to \infty$ are shown as well. Note that all the temperatures here are in °C, while the corresponding absolute temperatures (in K) are involved in eq 11 (see also the note below eq 6).

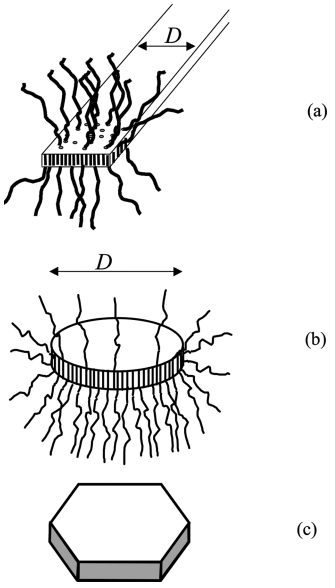

Figure 6. (a) A tapelike micelle with core of width D. (b) A disklike micelle with core of diameter $D = 2R_d$. (c) A possible hexagonal shape of the core.

the infinite lamellae must be replaced by less extended micelles.

As the layer motif is prescribed by crystallization of stereoregular fragments, we expect that micellar cores must still be parts of lamellar crystals with finite lateral size (at least along one dimension). The following two most symmetric micellar morphologies of that sort will be considered: tapelike micelles (Figure 6a) and disklike micelles (Figure 6b). Note that such micellar geometries are commonly found in solutions of amphiphilic molecules, in particular, tapes in peptide solutions[9] or in organogelators,[73,74] and disks in rod−coil copolymers,[77] associating polymers and ionomers,[78−80] and in coil−coil block copolymers in the so-called superstrong segregation regime.[76,75]

Both in the tapelike and disklike structures the conformational elastic energy is strongly reduced due to a divergence of chain trajectories (larger available space) in the corona region. These effects are considered quantitatively below.

There are two free energy terms to take care of: the edge energy of the core and the conformational energy. The edge energy is just proportional to the perimeter of the micelle core (the perimeter is $2\pi R_d$ for a disklike micelle of radius R_d). Strictly speaking, a disklike micelle is not exactly circular as the crystalline core is anisotropic, and its structure defines preferred directions for the edge. There are six equivalent lateral orientations of the edge in the case of the simple hexagonal symmetry of the crystals, so a hexagonal lateral shape can be expected (see Figure 6c).[81] The free energy difference between circular and hexagonal disklike micelles is just minute (around 5%), so the circular approximation is adopted below. (The effects due to more complicated crystalline core anisotropy are not considered here.)

3.3.1. Conformational Energy of Micellar Corona, $\tilde{H} \gg D$. Let us start with the asymptotic regime of long chains when the tape width (or the disk diameter) D is much larger than the core thickness H, while the characteristic corona height $\tilde{H} = \tilde{L}(N - n)$ is much longer than D: $\tilde{H} \gg D \gg H$. These conditions imply that $N \gg n$, so $\tilde{H} \simeq \tilde{L}_1 N$. The elastic energy of strongly stretched polymer chains in the corona (shell of a micelle) can be calculated "asymptotically exactly" in this regime for the Gaussian elasticity model using the electrostatic analogy established in ref 61. In this approach a formal unit electric charge is associated with those ends of amorphous polymer fragments that are adjacent to the crystallized segments (i.e., are located at the core surface). The coarse-grained chain trajectories in the shell follow the force lines of the formal electric field, and the local chain tension at any point in the shell is proportional to the electric field E. The total conformational elastic energy of the shell $\mathcal{F}_{conf}$ is proportional to the formal electrostatic energy $E_{el} = (8\pi)^{-1}\int E^2\, d^3r$: $\mathcal{F}_{conf} = CE_{el}$, where the coefficient $C = 3\upsilon k_B T/(4\pi b^2)$, and $\upsilon = M_1/(N_A\rho_m) = A_1 L_1 \rho_c/\rho_m$ is the volume per chemical unit in the shell. The problem is thus reduced to calculation of the electrostatic energy of a uniformly charged tape or disk (as the core thickness can be neglected).

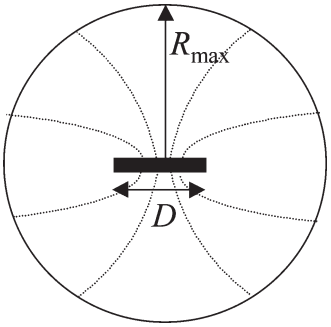

Figure 7. Corona of a micelle with tapelike core of width D; R_{max} is the corona radius.

3.3.2. Tapes for $\tilde{H} \gg D$. In the case of tapes the electrostatic energy is logarithmically diverging at long distances, so an N-dependent cutoff R_{max} must be introduced (Figure 7). R_{max}, the outer radius of the micelle (which is nearly cylindrical as a whole), is defined geometrically: The volume (per unit length along the main axis) occupied by the chains is $V = N\upsilon Q$ (here $Q = D/A_1$ is the total number of chains in the aggregate per unit length). υ must be equal to πR_{max}^2; hence $R_{max} = [DN\upsilon/(\pi A_1)]^{1/2}$. Thus

$$\frac{R_{max}}{\tilde{H}} = \left(\frac{2}{\pi}\frac{D}{\tilde{H}}\right)^{1/2} \tag{16}$$

Note that R_{max} for tapes (in the regime $D \ll \tilde{H}$) is much longer than D, but it is much shorter than the shell thickness $\tilde{H}$ for infinite lamellar micelle: $\tilde{H} \gg R_{max} \gg D$. The formal electrostatic energy (per unit length of uniformly charged tape) is

$$E_{el} \simeq Q^2\left(\ln\frac{R_{max}}{D} + \frac{3}{2}\right) \tag{17}$$

Thus, the shell free energy per chain is

$$F_{conf} \simeq CE_{el}/Q \simeq F_0\frac{\overline{D}}{2\pi}\left(\ln\frac{2}{\pi\overline{D}} + 3\right) \tag{18}$$

where $F_0 \equiv {}^3/_2 k_B T\tilde{H}^2/(\tilde{N}b^2)$ is the "reference" conformational energy per chain in the infinite lamellar micelle (see eq 9), and $\overline{D} = D/\tilde{H}$ is the reduced tape width.

3.3.3. Disks for $\tilde{H} \gg D$. The electrostatic energy of a thin uniformly charged disk (of radius $R_d = D/2$, total charge Q) is $E_{el} = 8Q_2/(3\pi R_d)$. For finite large N we must introduce the cutoff distance R_{max} (see Figure 7) defined by the geometrical condition (compare with the tape case) $4\pi R_{max}^3/3 = N\upsilon Q$, where $Q = \pi R_d^2/A_1$. Hence

$$\frac{R_{max}}{\tilde{H}} = \left(\frac{3}{2}\right)^{1/3}\left(\frac{R_d}{\tilde{H}}\right)^{2/3} \tag{19}$$

As before, $\tilde{H} \gg R_{max} \gg R_d$. The corrected for the cutoff electrostatic energy is

$$E_{el} \simeq Q^2\left(\frac{8}{3\pi}\frac{1}{R_d} - \frac{1}{2R_{max}}\right) \quad (20)$$

The conformational free energy per chain therefore is

$$F_{conf} \simeq CE_{el}/Q \simeq F_0\overline{R}_d\left[\frac{8}{3\pi} - (\overline{R}_d/12)^{1/3}\right] \quad (21)$$

where $\overline{R}_d = R_d/\tilde{H}$.

3.3.4. Comments on Conformational Energy. Equations 18 and 21 define F_{conf} for $D \ll \tilde{H}$. To consider a transition between say infinite lamellar layers and tapes, it is necessary to find F_{conf} also for $D \gtrsim \tilde{H}$. One simple "natural" idea is to assume that the polymer chains still follow the same trajectories as in the limit $N \rightarrow \infty$ (i.e., the chains are stretched along the electric force lines considered above). Unfortunately, this approximation is very poor for $D \gtrsim \tilde{H}$. In fact, the conformational energy per chain calculated using this approximation does not tend to that for infinite lamellar structure even in the limit $D \rightarrow \infty$ (when tapes or disks become physically equivalent to lamellae). A calculation for a disk with $D \gg \tilde{H}$ shows that the approximation overestimates F_{conf} by more than 40% (the ratio of approximate and exact energies is $1 + 4/\pi^2$). It is therefore clear that the edge part of F_{conf} cannot possibly be resolved with this approximation. (It also suffers from the following artifact: the chain tension is diverging near the disk or tape edge, which is highly unfavorable in the case of short chains.)

As an alternative solution one may try to seek for an "exact" elastic energy F_{conf} for finite $D/\tilde{H}$.[83] The "exact" asymptotic problem is formulated in Appendix A. The general problem is quite complicated for two reasons:

(i) The outer surface of the micelle (bounding the corona) is not known, so the free energy minimization with respect to its shape must be performed.

(ii) The electrostatic analogy does not hold in the general case. Instead, the problem can be mapped to a fluid flow problem for an inviscid incompressible fluid. The flow is not irrotational: it is characterized by an unknown bulk distribution of vorticity. Therefore, the "hydrodynamic" analogy does not help much since fluid mechanics of such flows is not as well-developed as for other flow types. The problem (concerning flow with vorticity and with unspecified bounding surface) is likely to be intractable analytically, and even its numerical treatment seems to be quite involved.

We therefore tend to resort to an approximate treatment. Specifically, we assume that all (coarse-grained) chain trajectories in the shell are straight lines. This approximation is certainly valid for a lamellar structure (where the chains are all stretched normal to the layer), so it is likely to work well for $D \gg \tilde{H}$. Below we show that the approximation is good also in other regimes (for $D \ll \tilde{H}$).[84]

The elastic free energy contributions for tape and disk structures are derived and minimized in Appendices B and C. The results obtained there are used in the next section. Note that the chain orientations and the chain tension distributions (along the chain contour) are not prescribed but rather are defined naturally by the minimization condition (in combination with the incompressibility condition). Note also that we still assume that the free chain ends are located at the outer surface of the micelle (the Alexander−de Gennes approximation).

4. Micelles in Homopolymer Melts: Phase Diagrams

4.1. Transitions Involving Nonlamellar Micelles. *4.1.1. Transition Lamellae → Tapes*. The free energy per chain in the tapelike aggregate (of width D, total length along the main axis $\mathscr{L}, \mathscr{L} \gg D$) is

$$F_{tape} = F_{lam} + \Delta F_{conf} + F_{edge} \quad (22)$$

where F_{lam} is the reference energy for lamellar micelle (see eq 4), $\Delta F_{conf} < 0$ is the shell energy decrement due to lower chain elongation near the tape edge, and $F_{edge} > 0$ is the free energy due to interfacial tension at the edge of the core. The tape conformational energy is considered in Appendix B:

$$\Delta F_{conf} \simeq F_0\frac{2W}{\overline{D}}$$

where W is defined in eqs B10 and B16 and $\overline{D} = D/\tilde{H}$. The total core-edge energy is

$$\mathscr{F}_{edge} = 2\gamma_e H\mathscr{L} \quad (23)$$

where γ_e is the surface tension at the core edge. Therefore

$$\frac{F_{edge}}{k_BT} = \frac{\mathscr{F}_{edge}A_1}{k_BTD\mathscr{L}} = 2J_e\frac{nL_1}{D} \quad (24)$$

where

$$J_e \equiv \frac{\gamma_e A_1}{k_BT} \quad (25)$$

The equilibrium tape free energy is

$$F_{tape} = F_{lam} + \min_D(\Delta F_{conf} + F_{edge})$$

Therefore

$$\frac{F_{tape} - F_{lam}}{F_0} = \min_{\overline{D}}\left(\frac{2W}{\overline{D}} + \frac{2\overline{J}}{\overline{D}}\right) \quad (26)$$

where

$$\overline{J} \equiv \frac{J_e nL_1}{F_0\tilde{H}} = \frac{2}{3}\frac{b^2L_1nJ_e}{\tilde{L}_1^{\,3}(N-n)^2} \quad (27)$$

The transition from infinite layers to tapes is defined by the condition $F_{tape} = F_{lam}$, i.e.

$$\min_{\overline{D}}\left(\frac{2W}{\overline{D}} + \frac{2\overline{J}}{\overline{D}}\right) = 0$$

leading to

$$\overline{J} = -\min_{\overline{D}} W = |W_0| \approx 0.498 \quad (28)$$

Tapes are stable for $\overline{J} < \overline{J}_{lt} = |W_0|$ (long enough chains).

Thus, the transition from infinite lamellar layers to tapes takes place as the parameter $\overline{J}$ is decreased below a certain value. This transition can be induced by a reduction of the edge energy (γ_e, J_e), but also by increasing the chain length N (see definition of $\overline{J}$, eq 27). The physical meaning of these results is simple: while a decrease of the edge tension makes

the tapelike micelle more stable (its free energy decreases), an increase of N results in a destabilization of the infinite sheet morphology in favor of tapelike micelle since larger N corresponds to higher shell conformational energy penalty which is partially relieved upon transition to a lower-dimensional tapelike structure.

The tape width is defined by the minimization of $[\overline{J} + W(\overline{D})]/\overline{D}$ with respect to $\overline{D}$. For $\overline{J}$ slightly below the threshold, $\overline{J} = |W_0|(1 - \varepsilon)$, $\varepsilon \ll 1$, we get using eq B18:

$$D \simeq \frac{2}{\sqrt{3}}\tilde{H}\ln(1/\varepsilon) \tag{29}$$

Therefore, the tape width diverges logarithmically near the transition point.

4.1.2. Transition Disordered Melt → Tapes. The transition line is defined by $F_{\text{tape}} = F_{\text{dis}} = 0$, where

$$F_{\text{tape}} \simeq \Delta F_{\text{cryst}} + F_{\text{entr}} + F_{\text{face}} + F_{\text{conf}} + F_{\text{edge}} \tag{30}$$

is the free energy per aggregated chain. The first three terms in the right-hand side of this equation are defined in eqs 6, 7, and 8. These terms do not depend on the tape width D. The last two terms are D-dependent: $F_{\text{conf}} = F_0(1 + 2W/\overline{D})$, where W is defined in Appendix B; F_{edge} is defined in eq 24.

4.1.3. Transition Tapes → Disks. The free energy per chain of a disklike micelle is

$$F_{\text{disk}} = F_{\text{lam}} + \Delta F_{\text{conf}} + F_{\text{edge}} \tag{31}$$

where ΔF_{conf} is the "excess" conformation energy for disks (with the reference to the conformational energy, $= F_0$, for an infinite layer). Using eq C8 leads to

$$\Delta F_{\text{conf}} = F_0(\overline{U} - 1) \tag{32}$$

where $\overline{U} = \overline{U}(\overline{R}_{\text{d}})$ is calculated in Appendix C. The edge energy is

$$F_{\text{edge}} = \frac{A_1}{\pi R_{\text{d}}^2}\gamma_{\text{e}} L_1 n 2\pi R_{\text{d}} = k_{\text{B}}T\frac{2L_1 n}{R_{\text{d}}}J_{\text{e}} \tag{33}$$

(compare with eq 24). Thus the reduced excess free energy for disks is

$$\frac{F_{\text{disk}} - F_{\text{lam}}}{F_0} = \min_{\overline{R}_{\text{d}}}\left(\overline{U} - 1 + \frac{2\overline{J}}{\overline{R}_{\text{d}}}\right) \tag{34}$$

The transition between tape and disk morphologies is defined by the condition $F_{\text{disk}} = F_{\text{tape}}$ which means that the rhs of eqs 34 and 26 must be equal. This happens at

$$\overline{J} = \overline{J}_{\text{td}} \approx 0.085$$

The disks are stable for $\overline{J} < \overline{J}_{\text{td}}$; the tapes are favored for $\overline{J} > \overline{J}_{\text{td}}$. The reduced tape width $\overline{D}$ and the disk radius $\overline{R}_{\text{d}}$ at the transition point are

$$\overline{D} \approx 0.780, \quad \overline{R}_{\text{d}} \approx 0.735$$

4.1.4. Transition Disordered Melt → Disks. This transition line is defined by the condition $F_{\text{disk}} = 0$, where F_{disk} can be obtained using eq 34 (F_{lam} there is defined in eq 4).

4.2. Phase Diagrams for PS. Semicrystalline micelles can be formed in principle at any T below the ideal crystallization temperature T_{m} of the corresponding stereoregular homopolymer (see Figure 4). That is why the range between T_{g} and T_{m} can be called the micelle (or cluster) window. However, it is important that at higher T's within this windows a thick crystalline core is required for micelle stability, so the volume fraction of stable micelles becomes extremely small rendering them undetectable as T is increased. Considering the phase diagrams (involving micelles of different types), it therefore appears natural to demand that the volume fraction of micelles ϕ is equal or exceeds some threshold ϕ^* (note that ϕ is related to the core thickness nL_1 via eq 3). More precisely, we consider the case of fixed $\phi = \phi^*$ since the micelles with lower ϕ are always formed first and since the transition lines separating the regions of different micellar geometries are nearly independent of ϕ (i.e., of n). By virtue of eq 3 the condition $\phi = \phi^*$ defines the length $n = n^*$ of the relevant stereoregular fragments (for a given degree of tacticity). Qualitatively, the phase diagrams do not depend much on ϕ^*; $\phi^* = 10^{-4}$ is chosen below (this value corresponds to the estimate obtained in a light scattering study[88]).

The micelle diagrams for PS are shown in Figures 8−10; the coordinates are reduced temperature T/T_{m} vs

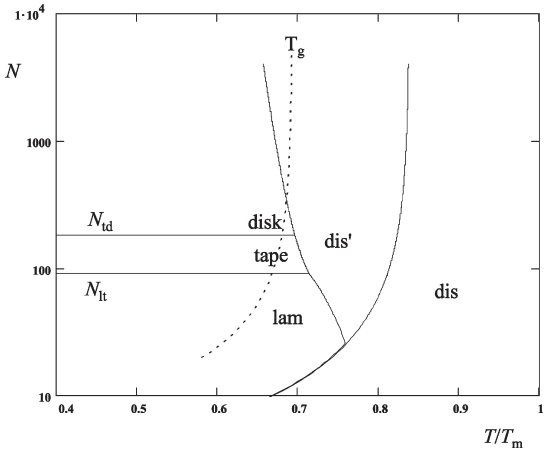

Figure 8. A phase diagram for PS melt: T/T_{m}, the reduced temperature; N, the polymerization degree. The degree of tacticity is $d_{\text{t}} = 1/3$; the reference volume fraction of micelles is $\phi^* = 10^{-4}$. Solid lines correspond to transitions between different regimes: dis (disordered melt); dis′ (micelles are formed but their volume fraction is less than ϕ^*); lam (lamellar micelles); tape (tapelike micelles); disk (disklike micelles). The dashed line (marked T_{g}) shows the glass transition temperature.

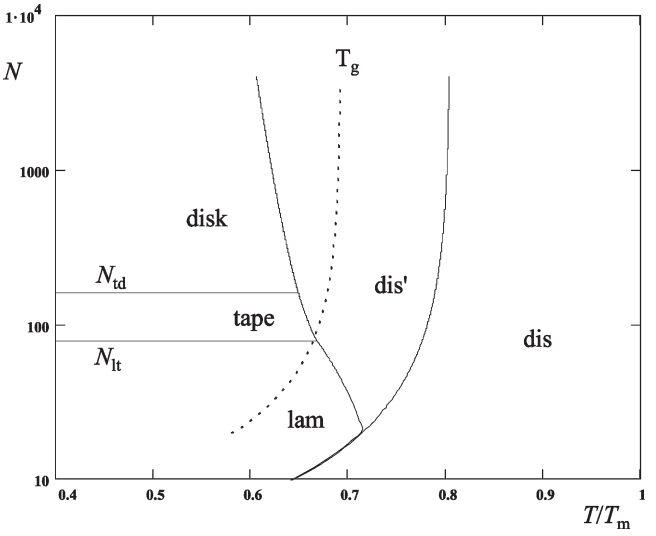

Figure 9. Same as Figure 8, but for $d_{\text{t}} = 0.2$.

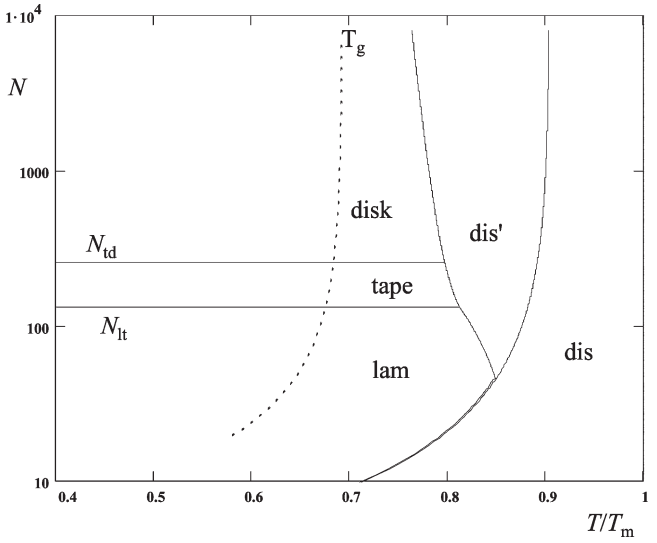

Figure 10. Same as Figure 8, but for $d_t = 0.6$.

polymerization degree N. The three diagrams correspond to different values of the degree of tacticity, $d_t = 1/3$, 0.2, 0.6, respectively. The parameters S_m and J_0 for PS are defined in eq 15. The parameter J_e is not known; it was assumed to be close to J_0: $J_e = 2$ (in other words, we assume that the surface tension at the crystal edge is similar to that of its faces). There are five regions separated by solid lines in each diagram: dis (disordered melt, no clusters); dis′ (clusters can be formed, but their volume fraction is lower than ϕ^*); lam (infinite lamellar layers); tape (tapelike micelles of infinite length); disk (disklike micelles). The dis → dis′ and dis (or dis′) → lam transitions were already discussed (see Figure 5). A crystal core thicker than the total contour length of a polymer chain is not allowed; hence, it is set $n = N$ for $N < n^*$ and $n = n^*$ for $N > n^*$. The widest T-window of lamellar micelles thus corresponds to $N = n^*$. Short chains, $N < n^*$, crystallize at lower T, while longer chains ($N > n^*$) form thicker amorphous corona increasing the conformational energy penalty for micelle formation.

Wide lamellar layers (platelets) become thermodynamically less favorable than tapelike and disklike micelles in the long-chain regime. To see this, let us recall that the shell contribution to the micelle free energy per aggregated chain (the conformational energy F_{conf}) strongly increases with the chain length being nearly proportional to N in the lamellar micelle regime (see eq 9). The dependence of F_{conf} on N is much weaker for tapelike micelles (of fixed width D): the energy increase is only logarithmic there (see eq 18). Finally, for disklike micelles (of fixed radius R_d) the corresponding increase is even more weak since F_{conf} does not grow indefinitely, but rather saturates as $N \to \infty$ (see eq 21). Therefore, a lot of conformational energy can be relaxed for large N upon transitions from lamellar platelets to tapes and then to disks.

The transitions lam → tape and tape → disk occur as N increases, at $N = N_{lt}$ and $N = N_{td}$, respectively. The main parameters for the diagrams shown in Figures 8−10 are

$$d_t = 1/3, \quad \Delta\varepsilon \approx 0.7, \quad n^* \approx 25, \quad N_{lt} \approx 91, \quad N_{td} \approx 183$$

$$d_t = 0.2, \quad \Delta\varepsilon \approx 0.41, \quad n^* \approx 20, \quad N_{lt} \approx 79, \quad N_{td} \approx 161$$

$$d_t = 0.6, \quad \Delta\varepsilon \approx 1.4, \quad n^* \approx 45, \quad N_{lt} \approx 132, \quad N_{td} \approx 256$$

The crystalline core lamellar thickness for $d_t = 1/3$ is $H \approx nL_1 \approx 5.5$ nm (for $N > 25$). The transition from infinite lamellae to tapes is continuous; the width D of crystalline core of a tape is infinite at the transition point $N = N_{lt}$; the tape width decreases at larger N down to $D \approx 0.78(N - n^*)\tilde{L}_1 \approx 15$ nm at $N = N_{td}$. Just above N_{td} the disklike micelles with crystalline core of radius $R_d \approx 0.735(N - n^*)\tilde{L}_1 \approx 14$ nm are formed; the radius decreases asymptotically tending to

$$R_d \approx 1.2b(L_1 n J_e/\tilde{L}_1)^{1/2} \tag{35}$$

i.e. to $R_d \approx 8$ nm as N is further increased.

The dashed lines in Figures 8−10 show the glass-transition temperature. A tendency for cluster formation is expected also below T_g, although an equilibrium cluster structure is not accessible in this region.

The width of the T-window of the micelle regimes (above T_g) strongly depends on the degree of tacticity d_t: the micelle regions are wider for higher d_t. The regions of tapes and disks (above T_g) disappear at low d_t. The micelle T-window also decreases (shrinks) at high molecular weights, M. For high $M \gtrsim 10^5$−10^6 stable micelles are predicted if d_t is significantly higher than 1/3 (for example, for $d_t = 0.6$, see Figure 10), which is not typical for conventional atactic PS. These results perhaps explain why cluster effects in PS melts were observed rheologically (low-f elasticity), but not in the light scattering experiments (i.e., low-q excess scattering was not detected for neat PS). The reason is related to the difference of molecular weights. Rather short PS chains ($M \approx 4000$) were involved in rheological studies;[20] the corresponding T-window of lamellar crystals is rather wide in the predicted diagrams (Figures 8 and 9). On the other hand, PS samples of much larger molecular weight ($M \gtrsim 2 \times 10^5$) were studied by light scattering (see refs 14 and 89 and references therein); micelles are not predicted for such long chains (see Figures 8 and 9).

5. Discussion and Conclusions

1. In this paper we show that thermodynamically stable finite aggregates (semicrystalline micelles) can be formed in melts of homopolymers if they are stereoisomeric. The idea is that generally atactic (stereoirregular) polymers still contain some rather long stereoregular segments. These rare fragments can aggregate and form a lamellar crystal serving as a micelle core surrounded by a shell of noncrystallizable (amorphous) parts of the chains (see Figure 3b). Thus, the aggregates are core/shell structures formed by atypical polymer chains containing sufficiently long stereoregular fragments. The cluster formation therefore bears some similarity to micellization in block copolymers.[61,56,76,32,8]

The lamellar micelles can be stable below the limiting temperature T^* (see eq 11) which increases with the degree of tacticity d_t. T^* approaches T_m (the ideal crystallization temperature for undiluted *stereoregular* isomer of the same polymer) at high d_t, so, in principle, micelles can be formed at any T below T_m.

2. The relevant stereoregular fragments are isotactic if meso diads dominate over racemo diads, $\Delta\varepsilon > 0$; syndiotactic fragments are dominating in the opposite case. The latter (syndiotactic) case applies for conventional PS: $f_m < 0.5$, $\Delta\varepsilon < 0$. Nevertheless, it is the case $\Delta\varepsilon > 0$ that was considered in the present paper. This is appropriate for illustrative purposes since (i) the probability of a stereoregular fragment depends on the magnitude of $\Delta\varepsilon$ (the sign does not matter) and (ii) the relevant properties of isotactic PS are known with better confidence as compared with the syndiotactic PS. Note that crystallization temperature T_m is higher for syndiotactic PS than for isotactic PS, so an even wider "cluster T-window" may be expected in the syndiotactic case.

3. The theory of semicrystalline micelle formation developed in the present paper involves three approximations related to the

calculation of elastic energy of strongly stretched chain parts in the shell: We assumed that (i) neighboring chains in the shell are elongated in a similar way (Alexander−de Gennes approximation); (ii) the chains are characterized by ideal (Gaussian) elasticity; (iii) the smoothed chain trajectories in the shell are straight lines. Let us consider the typical errors associated with these approximations for the two limiting cases: (1) infinite lamellar layer; (2) disklike micelle with very long tails in the corona. In the first case, the approximation (i) overestimates the conformational (elastic) free energy by ≈22% and approximation (ii) underestimates the elastic energy by ≈10% (see section 3.1.3), and the last approximation is exact. In the second case, the first approximation is exact, approximation (ii) underestimates the energy by less than 10% (as the chains are less stretched in the corona of a disklike micelle than in the laterally infinite plain brush with the same grafting density), and the last approximation overestimates the elastic energy by ≈8.5%. Thus, in all the cases the errors due to the approximations are partially compensated, and the resultant error does not exceed 12%.

4. The theory of the crystalline micelle core involves the following important parameters: T_m, the ideal crystallization temperature of stereoregular polymer, S_m, the corresponding entropy of melting per monomer unit, and J_0, the reduced energy of crystal face. All these parameters are obtained by extrapolation of the relevant crystal melting data. As we argue in section 3.2.3 the obtained parameters T_m and S_m are probably underestimated, while J_0 is overestimated for PS. All these inaccuracies work against micelle formation, so that actual region of their stability is perhaps wider than that predicted here.

5. The theory provides a basis for explanation of anomalous low-frequency rheological phenomena (solidlike behavior in macroscopic gaps between solid surfaces) observed in certain polymer melts.[20−23,25,27] Indeed, it looks like that all the homopolymers exhibiting the low-frequency elasticity are stereoisomeric, including PS,[20] poly(*n*-butyl acrylate),[22,21] 1,4-polybutadiene,[21] and poly(propylene glycol)[27] (liquid-crystalline polymers are omitted here). The molecular weight of the rheologically studied polymers was not very high, ranging from $M = 4000$ (PS, PPG) to 26 000 (PBuA). Therefore, we can expect formation of lamellar micelles in these polymer melts. Such semicrystalline micelles (being theoretically infinite) can reach lateral size of many micrometers. Therefore, the micelles can possibly bridge a macroscopic gap between solid surfaces confining the polymer layer. It is important that the low-frequency elasticity was detected only when the confining surfaces were treated in a special way. The idea is that such treatment renders the surfaces attractive for the lamellar edges, so that weak bonds can be formed between the edges and the surfaces. Hence, lamellae can serve as bridges (Figure 11). Such highly rigid (semicrystalline!) bridging layers would certainly give rise to an apparent solidlike shear response of the confined polymer melt. The fact that the volume fraction of micelles is very low (say, $\phi < 10^{-3}$ [88,90]) can be compensated by very high elongational elastic modulus of their crystal core, thus giving rise to a considerable (measurable) apparent modulus of the melt.

In addition, the combination of weak surface bonds and high rigidity of the bridging layers must result in a strongly nonlinear elastic response: the shear elastic modulus must significantly decrease with shear amplitude γ already for small strains. This is in agreement with experimental data indicating that the linear regime of low-frequency elasticity is limited to $\gamma < 0.1-0.5\%$.[22,21]

6. The predicted mechanism of micelle formation may be responsible for anomalous low-q excess scattering observed in certain polymer melts (Fischer clusters). In particular, it may be relevant to cluster phenomena in PMpTS[11−13] and PLMA[14] which are both stereoisomeric.

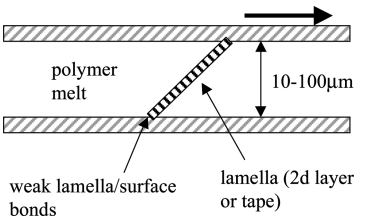

Figure 11. Confined polymer layer and a bridging lamellar micelle.

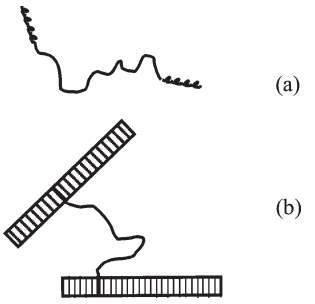

Figure 12. (a) A polymer chain with two stereoregular fragments. (b) Two disklike micelles connected by such bridging chain.

7. As was mentioned above, an anomalous low-q scattering was never observed in PS melts. Still cluster modes were found in PS solutions in toluene ($M \sim 10^5$, concentration $c \approx 12-25\%$, room T).[88,90] Toluene is a good solvent for PS, so cluster formation is puzzling. We suggest that it may be driven by the general mechanism proposed in this paper (aggregation and crystallization of atypical stereoregular chain segments). This idea is supported by the experimental evidence that stereoregular PS tends to crystallize in toluene forming stable complexes with solvent molecules (1:0.8 intercalates).[92] This complex compound is stable up to ca. 120 °C. The intercalated structure is more stable than a neat PS crystal; hence, the regions of micelle stability in the PS solutions must be shifted to higher temperatures as compared to the melt case (in other words, the transition lines in the phase diagram, see Figure 8, must be shifted to the right), so that semicrystalline micelles may become stable even at high M.

8. Cluster modes were observed in PS of rather high molecular weight: $M \sim 10^5$, $N \sim 10^3$ (see the previous point). This PS chain length certainly falls into the regime of disklike micelles. Other polymers showing anomalous low-q excess scattering also have rather high molecular weights ($M \approx 10^5$ for PLMA, $M \approx 15\,000$ for PMpTS) probably corresponding to the same regime. (It is hard to be more precise as the illustrative phase diagrams, Figures 8−10, apply to PS.) The predicted disk-core thickness is $H \lesssim 6$ nm, and its diameter is $2R_d \lesssim 30$ nm. These size parameters are much smaller than the cluster size $\xi \sim 100-300$ nm obtained by both static and dynamic light scattering.[12,88]

A tentative explanation of this discrepancy is considered below: Some of the polymer chains may contain two stereoregular fragments rather than just 1 (Figure 12a). These chains can form bridges between neighboring micelles (Figure 12b). The relative fraction of such chains is $p_{br} \sim \phi/2$ (see eq 3). The bridging attraction energy is proportional to the number of bridges Qp_{br}. Therefore, it is possible that disklike micelles can aggregate and form larger clusters as long as Qp_{br} is large enough.

This mechanism does not apply to infinite lamellar and tapelike micelles since they are protected by shell layers of strongly stretched "tails" which do not allow micelles to come close to each other. As a result, a bridging chain has to stretch a lot; the bridge formation is suppressed as a result. By contrast, well in the regime of disks the outer parts of amorphous tails are not strongly stretched, so the elastic energy penalty for bridging is low.

The argument can be developed more quantitatively. The shell of a disklike micelle is similar to that of a block copolymer spherical micelle: generally it consists of a proximal part (coat) of radius R_{coat} where tails are strongly stretched and the distal outer part where the chains are weakly perturbed (nearly Gaussian).[61] The bridging is not suppressed if

$$R_{coat} \lesssim R_{coil} = \tilde{N}^{1/2} b \tag{36}$$

where R_{coil} is the Gaussian polymer coil size (note that $\tilde{N} \approx N$ as $n \ll N$ in the regime of disks). This condition is equivalent to

$$3Q/(4\pi) \lesssim \tilde{N}^{1/2} b^3/v$$

where $Q = \pi R_d^2/A_1$ is the micelle aggregation number. On using eq 35, the latter condition leads to $N \gtrsim 600$.

The picture of clusters involving many micelles also explains why depolarized (VH) light scattering does not show any significant low-q excess intensity:[12,14] It is expected that disklike micelles are oriented randomly in a cluster thus giving rise to incoherent VH scattering of individual micelles which is much weaker than coherent VV scattering of the whole cluster.[93]

9. The proposed theory of semicrystalline micelle formation naturally leads to low volume fraction ϕ of clusters in qualitative agreement with light scattering and spin-echo experiments[88,90] pointing to $\phi \sim 10^{-3}-10^{-4}$. Low ϕ explains why cluster contribution to the bulk viscosity was not detected rheologically.[25] The clusters were never detected by WAXS, perhaps, for the same reason.

10. The theory also implies that the propensity to form clusters strongly depends on the degree of tacticity: an increase of d_t promotes micelle formation. Experimental studies of cluster effects on a series of similar polymer with different d_t are thus invited. In view of the diagram, Figure 10, it would be extremely interesting to synthesize atactic PS samples with high d_t (say, $d_t = 0.6$) and with molecular weights ranging from, say, $M = 3000$ to 10^6 and to study these samples by light scattering. More generally, continuous variation of the degree of tacticity may serve as an interesting route from glass-forming to crystallizable polymers.

11. It is therefore possible that both the rheological and the scattering anomalous phenomena in homopolymer melts (low-frequency elasticity and low-q scattering) are related to a crystallization rather than to the glass transition.[91]

So far, the rheological and light scattering studies are done on different sets of polymers. Complementary studies are thus invited (like light scattering of lower M PS).

12. The proposed mechanism of cluster formation in homopolymer melts is certainly quite universal. However, we do not claim that this is the only aggregation mechanism applicable to all cluster phenomena is homopolymers. Other effects may be involved, in particular, in the case of amphiphilic homopolymers.[14,94,95]

One important example of a system to which the proposed mechanism (based on stereoisomerism) is not applicable is provided by PEO. (It looks like PEO is the only homopolymer showing cluster phenomena which is not stereoisomeric.) It is worth noting that PEO is a rather special polymer. Typically, it forms clusters in solutions (in particular, in dilute aqueous solutions). Cluster modes in PEO *melts* were detected by light scattering;[16,96] however, we are not aware of any estimate of the typical cluster size in this polymer.

PEO is an amphiphilic and hygroscopic polymer capable of forming inter- and intramolecular hydrogen bonds mediated by water molecules. PEO is also crystallizable (semicrystalline) fiber-forming polymer. These features can be at the root of cluster phenomena in PEO. Clusters in PEO of $M = 5 \times 10^4$ were observed for $T > 65$ °C, just above the apparent melting temperature for this polymer, $T_m \approx 60$ °C.[16,96] It is possible that PEO can form several crystal structures and that its alternative crystal phase, which is less accessible kinetically, is stable above T_m. In this case, one can expect formation of solidlike domains at $T > T_m$, perhaps with very low nucleation rate, explaining low volume fraction of the crystallites. A growth of these alternative crystal structures can be limited by frustration effects[31,97] leading to a finite domain size.

Acknowledgment. I acknowledge stimulating discussions with I. A. Nyrkova.

Appendix A. Elastic Energy of a Polymer Brush Grafted to an Arbitrary Surface

Consider a layer of polymer chains (N chemical units of volume v, statistical segment b) grafted to a solid surface ($\mathcal{S}$) of arbitrary geometry (Figure 13). The number of chains per unit surface area is σ. The polymer medium is incompressible. All free chain ends are located on the outer surface ($\mathcal{F}$) whose shape is free (apart from the condition that the total volume $\mathcal{V}$ between the $\mathcal{S}$ and $\mathcal{F}$ surfaces is prescribed, equal to $Nv\int\sigma\, d\mathcal{S}$).

A smoothed chain trajectory $\mathbf{r}(n)$, $n = 1, ..., N$, depends on its grafting position $\mathbf{r}(0)$; the whole trajectories of two chains with close grafting points are also close to each other. It is therefore possible to introduce the field of chain tensions, $\boldsymbol{\tau} \equiv (3k_BT/b^2)(d\mathbf{r}/dn)$, which can be considered as a function of the position $\mathbf{r}$. The incompressibility condition dictates that

$$\nabla \cdot \boldsymbol{\tau} = 0 \quad \text{for } \mathbf{r} \text{ in } \mathcal{V} \tag{A1}$$

and that

$$\boldsymbol{\tau} \cdot \mathbf{n}_s = \frac{1}{\varkappa}\sigma \quad \text{for } \mathbf{r} \text{ on } \mathcal{S} \tag{A2}$$

where $\mathbf{n}_s$ is the unit vector locally normal to the solid surface, and $\varkappa \equiv b^2/(3vk_BT)$. The mechanical equilibrium in the bulk demands that

$$\varkappa(\boldsymbol{\tau} \cdot \nabla)\boldsymbol{\tau} - \nabla p = 0 \quad \text{for } \mathbf{r} \text{ in } \mathcal{V} \tag{A3}$$

where $p = p(\mathbf{r})$ is the pressure field. As for the outer (free) surface ($\mathcal{F}$), there are two forces acting on an element of the surface: the pressure force which is normal to the surface and the tension force along the chain trajectory. The force balance (implied by the equilibrium state) thus leads to two conditions: (i) chain trajectory must be locally perpendicular to the free surface, or

$$\boldsymbol{\tau} = \text{const}\, \mathbf{n}_f \quad \text{for } \mathbf{r} \text{ on } \mathcal{F} \tag{A4}$$

where $\mathbf{n}_f$ is normal to the free surface and (ii)

$$\varkappa\tau^2 = p \quad \text{for } \mathbf{r} \text{ on } \mathcal{F} \tag{A5}$$

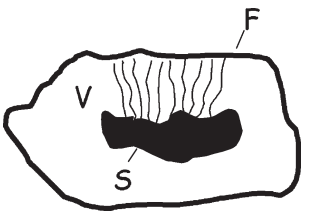

Figure 13. An incompressible layer $\mathcal{V}$ of polymer chains grafted to the solid surface S; the free chain ends are at the outer surface $\mathcal{F}$.

(for simplicity, it is assumed that $p = 0$ outside the micelle). In addition, it is necessary to demand that each chain comprises exactly N units, i.e., that for each point $\mathbf{r}_0$ on $\mathcal{S}$

$$\frac{1}{\varkappa v}\int \frac{\mathrm{d}r}{\tau} = N \tag{A6}$$

where the integral must be taken from $\mathbf{r}_0$ to the free surface along the line everywhere tangential to $\boldsymbol{\tau}$.

Equations A1 and A3 and the boundary conditions A2, A4, and A5 define the chain trajectories, while eq A6 defines the shape of the free surface. Once these equations are solved, the elastic conformational energy can be found:

$$\mathscr{F}_{\mathrm{conf}} = \frac{\varkappa}{2}\int_{\mathscr{V}} \tau^2\, \mathrm{d}^3 r \tag{A7}$$

The "bulk" eqs A1 and A3 are formally analogous to dynamical equations for incompressible inviscid fluid, with fluid pressure $-p$, velocity $\boldsymbol{\tau}$, and density $\varkappa$. In particular, one can find (in analogy with the Bernoulli equation)

$$\boldsymbol{\tau} \times (\nabla \times \boldsymbol{\tau}) = \nabla\varphi \tag{A8}$$

where $\varphi = \tau^2/2 - (1/\varkappa)p$, showing that φ is constant along the chain trajectory. It is important, however, that the flow is not irrotational in the general case ($\nabla \times \boldsymbol{\tau} \neq 0$): although the condition $\nabla \times \boldsymbol{\tau} = 0$ is compatible with eqs A1 and A3 and it specifies a family of their particular solutions, it is not possible to satisfy the free surface boundary conditions with this irrotational family.

Appendix B. Elastic Shell Energy for Tapelike Structures

Let us first consider a semi-infinite lamellar layer. The atactic chain parts are "attached" to the semi-infinite plane ($\mathscr{P}$) representing the core whose thickness is neglected. The chains are stretched along straight lines forming angle $\alpha = \alpha(y)$ with the surface, y is the distance to the edge along the surface, $\alpha(0) = 0$, $\alpha(\infty) = \pi/2$ (see Figure 14). The chains starting on the surface element ΔS_0 form a wedge $\mathscr{W}$; the wedge cross section (perpendicular to the chains) is $\Delta S(x)$, where x is the distance from the surface along the chain

$$\frac{\Delta S(x)}{\Delta S_0} = \sin\alpha + x\alpha' \tag{B1}$$

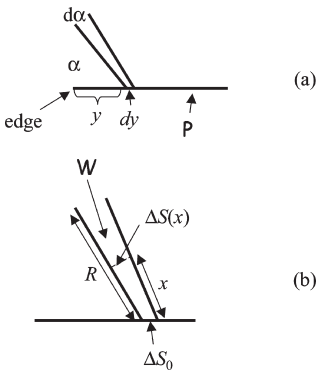

Figure 14. (a) The chain orientations in the shell near the core edge. $\mathscr{P}$ is the core surface, y is the distance of the "grafting" point to the edge, α is angle between the chain and the surface. (b) The wedge $\mathscr{W}$ formed by elongated chains starting at the surface element ΔS_0. R is the total chain length (end-to-end distance).

where $\alpha' \equiv \mathrm{d}\alpha/\mathrm{d}y$. The radial wedge length R is defined by the incompressibility condition

$$\int_0^R \Delta S(x)\, \mathrm{d}x = \Delta S_0 \tilde{H} \tag{B2}$$

(this equation was obtained having in mind the reference state: the infinite uniform brush of thickness $\tilde{H}$).

The chain tension is inversely proportional to $\Delta S(x)$: $\tau = [\Delta S_0/\Delta S(x)]\tau_{\mathrm{ref}}$, where $\tau_{\mathrm{ref}} = (3k_{\mathrm{B}}T/b^2)\tilde{L}_1$ corresponds to the reference state. The elastic energy of the ΔS_0 wedge therefore is

$$\mathscr{F}_{\mathrm{conf}}(\Delta S_0) = F_0 \frac{\Delta S_0}{2A_1}\int_0^R \frac{\mathrm{d}x}{\tilde{H}}\frac{\Delta S_0}{\Delta S(x)} \tag{B3}$$

Taking into account the wedges on both sides of the core, we get the total conformational energy:

$$\mathscr{F}_{\mathrm{conf}} = F_0 \int \frac{\mathrm{d}A}{A_1} I \tag{B4}$$

where $\int \mathrm{d}A$ is taken over the plane $\mathscr{P}$, $\mathrm{d}A = \mathscr{L}\mathrm{d}y$, where $\mathscr{L}$ is the edge length, and

$$I = I(y) = \int_0^R \frac{\Delta S_0}{\Delta S(x)}\frac{\mathrm{d}x}{\tilde{H}} \tag{B5}$$

Obviously, $I \to 1$ far from the edge (for $y \gg \tilde{H}$). The edge energy therefore is

$$\Delta\mathscr{F}_{\mathrm{conf}} = F_0 \frac{\tilde{H}\mathscr{L}}{A_1} W \tag{B6}$$

where

$$W = \int_0^\infty \frac{\mathrm{d}y}{\tilde{H}}(I(y) - 1) \tag{B7}$$

Using eqs B1 and B2 yields

$$\alpha' = \frac{2}{R^2}(1 - R\sin\alpha) \tag{B8}$$

The reduced length variables ($\overline{x} = x/\tilde{H}$, $\overline{R} = R/\tilde{H}$, $\overline{y} = y/\tilde{H}$) are used here and below in this Appendix, while the "overbar" signs are omitted (in other words, $\tilde{H}$ is considered as the unit length). Equations B5 and B1 lead to

$$I = \frac{1}{\alpha'}\ln\left(1 + \frac{\alpha' R}{\sin\alpha}\right) \tag{B9}$$

Substituting eqs B9 in eq B7, changing the integration variable, and using eq B8 gives

$$W = \int_0^{\pi/2} f\, \mathrm{d}\alpha,$$

$$f = f(\alpha, t) = \frac{1}{2\sin^2\alpha}\frac{t^2}{1-t}\left[\frac{1}{2\sin^2\alpha}\frac{t^2}{1-t}\ln\left(\frac{2}{t} - 1\right) - 1\right] \tag{B10}$$

where $t \equiv R\sin\alpha$. Note that t is a free variable (independent of α), so that the free energy minimization can be achieved by simply minimizing the integrand f with respect to t:

$$f(\alpha) = \min_t f(\alpha, t)$$

This yields the following equation

$$t^2\left(\frac{1}{1-t}\ln\left(\frac{2}{t}-1\right)-\frac{1}{(2-t)^2}\right)=\sin^2\alpha \qquad \text{(B11)}$$

which defines R, α' as a function of α. Both W and the function $\alpha(y)$ can be then obtained by integration:

$$W = W_0 \approx -0.49799 \qquad \text{(B12)}$$

As for $\alpha(y)$, it is singular at $y \to 0$ (with log-divergent derivative), while in the opposite limit ($y \gg 1$)

$$\alpha \simeq \frac{\pi}{2} - \exp\left(-\frac{y+y_0}{\xi}\right) - \frac{3\sqrt{3}}{4}\exp\left(-2\frac{y+y_0}{\xi}\right) \qquad \text{(B13)}$$

where $\xi = 2/\sqrt{3}$ and $y_0 \approx 0.884788$.

The case of tape of finite width ($0 < y < \overline{D} \equiv D/\tilde{H}$) can be considered in a similar way. The total conformational energy is (see eqs B4, B6, and B7):

$$\mathscr{F}_{\text{conf}} = F_0\frac{\mathscr{J}\tilde{H}}{A_1}(\overline{D}+2W) \qquad \text{(B14)}$$

where W is still formally defined in eq B10. The only difference is that now we must impose an additional condition:

$$\int_0^{\pi/2}\frac{d\alpha}{\alpha'} = \frac{\overline{D}}{2} \qquad \text{(B15)}$$

Minimization of W with additional condition B15 leads to

$$t^2\left(\frac{1}{1-t}\ln\left(\frac{2}{t}-1\right)-\frac{1}{(2-t)^2}\right)=\lambda\sin^2\alpha \qquad \text{(B16)}$$

where λ is related to the relevant Lagrange multiplier. This equation defines t as a function of α, λ; on substitution of the result in eqs B10, we get W as a function of λ. The dependence $W(\overline{D})$ is implicitly defined by this function and by the following equation defining how $\overline{D}$ depends on the parameter λ (as t depends on both α and λ):

$$\overline{D} = \int_0^{\pi/2}\frac{1}{\sin^2\alpha}\frac{t^2}{1-t}\,d\alpha \qquad \text{(B17)}$$

The plot of the reduced energy W vs $\overline{D}$ is shown in Figure 15. For $\overline{D} \gg 1$ the function $W(\overline{D})$ is well-approximated as

$$W \simeq W_0\left(1-\exp\left(-\frac{\sqrt{3}}{2}\overline{D}\right)\right) \qquad \text{(B18)}$$

where W_0 is defined in eq B12 (the error due to this approximation is less than 0.5% for $\overline{D} > 2$, see Figure 15). In the opposite regime ($\overline{D} \ll 1$) we get

$$\overline{D} + 2W \simeq \frac{\overline{D}^2}{2\pi}\ln\left(\frac{2\pi}{\overline{D}}\right) \qquad \text{(B19)}$$

The conformational energy *per chain* for $\overline{D} \ll 1$ is (see eq B14 and note that $\mathscr{J}\tilde{H}\overline{D}/A_1$ is the total number of chains in the tape)

$$F_{\text{conf}} = F_0(1+2W/\overline{D}) \simeq \frac{\overline{D}}{2\pi}\ln\left(\frac{2\pi}{\overline{D}}\right) \qquad \text{(B20)}$$

This result is in good agreement with eq 18.

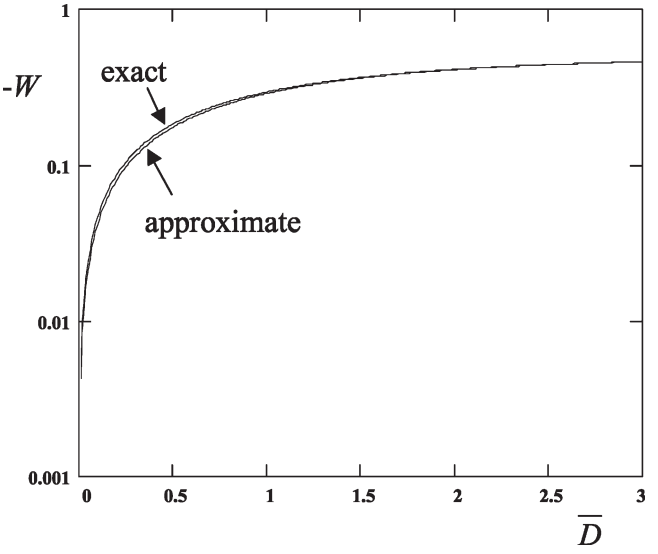

Figure 15. The reduced shell energy of a tape, W, vs the reduced tape width $\overline{D}$: exact (calculated using eqs B10 and B17) and approximate (eq B18).

Appendix C: Elastic Energy for Disklike Micelles

The conformational energy of disklike micelles can be calculated on the same footing as for tapes. As before the core thickness is neglected, so we consider monodisperse chain sections (degree of polymerization $N - n$) uniformly "grafted" to a disk of radius R_d. The grafting density is $1/(2A_1)$ on each side of the disk. Let us turn to the wedge picture (see Figure 14b). The ratio of cross sections is now

$$\frac{\Delta S(x)}{\Delta S_0} = (\cos\theta + \theta' x)\left(1+\frac{x}{r}\sin\theta\right) \qquad \text{(C1)}$$

where θ is the angle between the chain direction and the normal to the disk (thus $\theta = \pi/2 - \alpha$), r is the distance from the grafted end to the disk center, and $\theta' = d\theta/dr$. The total length of the 'grafted chain', R, is defined by the incompressibility condition:

$$\int_0^R \frac{\Delta S(x)}{\Delta S_0}\,dx = 1 \qquad \text{(C2)}$$

leading to equation

$$\frac{\sin\theta}{3rr'}R^3 + \frac{1}{2}\left(\frac{1}{r'}+\frac{\sin\theta\cos\theta}{r}\right)R^2 + R\cos\theta - 1 = 0 \qquad \text{(C3)}$$

where $r' \equiv dr/d\theta = 1/\theta'$. (Here and below we use the reduced lengths x, r, R considering $\tilde{H}$ as the unit length like in Appendix B.)

The total conformational energy is

$$\mathscr{F}_{\text{conf}} = K\int_0^{\overline{R}_d} 2\pi r I\,dr \qquad \text{(C4)}$$

where $K = F_0(\tilde{H}^2/A_1)$, $\overline{R}_d = R_d/\tilde{H}$, and

$$I = \int_0^R \frac{\Delta S_0}{\Delta S(x)}\,dx$$

(compare with eqs B4 and B5). Using eq C1 leads to

$$I = \frac{rr'}{r - r'\sin\theta\cos\theta}\ln\frac{1+\frac{R}{r'\cos\theta}}{1+\frac{R\sin\theta}{r}} \qquad \text{(C5)}$$

Changing the variable from r to θ in eq C4, we get

$$\mathscr{F}_{\mathrm{conf}} = 2\pi K \int_0^{\pi/2} \mathscr{L}\, \mathrm{d}\theta$$

where

$$\mathscr{L} = \mathscr{L}(r, r', \theta) = \frac{r^2 (r')^2}{r - r' \sin\theta \cos\theta} \ln \frac{1 + \frac{R}{r' \cos\theta}}{1 + \frac{R \sin\theta}{r}} \qquad \text{(C6)}$$

Here $R = R(r,r',\theta)$ is the only root (for $R > 0$) of the cubic eq C4. Upon solving this equation, an exact algebraic expression for R was substituted in eq C6. Minimization of $\mathscr{F}_{\mathrm{conf}}$ leads to Euler equation defining the second derivative of $r(\theta)$:

$$\frac{\mathrm{d}^2 r}{\mathrm{d}\theta^2} = \left(\frac{\partial \mathscr{L}}{\partial r} - \frac{\partial \mathscr{P}}{\partial \theta} - r' \frac{\partial \mathscr{P}}{\partial r} \right) \Big/ \frac{\partial \mathscr{P}}{\partial r'} \qquad \text{(C7)}$$

where $\mathscr{P} = \partial \mathscr{L} / \partial r'$. Solving eq C7 with initial condition $r'|_{\theta=0} = P$, we find numerically $r(\theta)$, $\overline{R}_{\mathrm{d}} = r(\pi/2)$, and $\mathscr{F}_{\mathrm{conf}}$, all as functions of the parameter P. The dependence of $\mathscr{F}_{\mathrm{conf}}$ on $\overline{R}_{\mathrm{d}}$ is implicitly defined as a result. In the general case

$$\frac{F_{\mathrm{conf}}}{F_0} = \frac{\mathscr{F}_{\mathrm{conf}}}{\pi \overline{R}_{\mathrm{d}}{}^2 K} = \overline{U}(\overline{R}_{\mathrm{d}}) \qquad \text{(C8)}$$

where $\overline{U}$ is a universal function of the reduced radius $\overline{R}_{\mathrm{d}}$. It is plotted in Figure 16, in variables $(1/\overline{R}_{\mathrm{d}} + 1)\overline{U} - 1$ vs $\overline{R}_{\mathrm{d}}{}^{1/3}$.

In the limit of small disk radius, $\overline{R}_{\mathrm{d}} \ll 1$, we get

$$\overline{U} \approx \frac{8}{3\pi} \overline{R}_{\mathrm{d}} (1.085 - 0.585 \overline{R}_{\mathrm{d}}{}^{1/3}) \qquad \text{(C9)}$$

Comparing this approximate result with the asymptotically exact eq 21, we see that the straight-chain approximation overestimates the conformational elastic energy by about 8% (or less) in this regime. (The approximate energy is of course higher since the exact result corresponds to the energy minimum.)

More precisely, the conformational energy for $\overline{R}_{\mathrm{d}} \ll 1$ can be approximated as

$$\overline{U} \simeq \frac{8}{3\pi} \overline{R}_{\mathrm{d}} (1.08531 - 0.58467 \overline{R}_{\mathrm{d}}{}^{1/3} - 0.03215 \overline{R}_{\mathrm{d}}{}^{2/3} - 0.003 \overline{R}_{\mathrm{d}}) \qquad \text{(C10)}$$

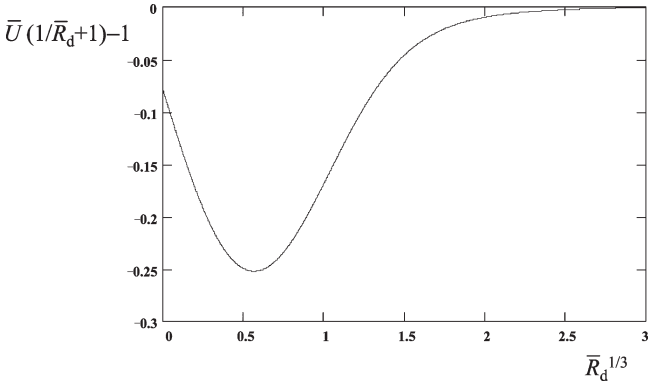

Figure 16. Dependence of the reduced elastic energy per chain, $\overline{U}$, in the shell of a disklike micelle on the reduced radius $\overline{R}_{\mathrm{d}}$ of its core: $(1/\overline{R}_{\mathrm{d}} + 1)\overline{U} - 1$ is plotted vs $\overline{R}_{\mathrm{d}}{}^{1/3}$.

For $\overline{R}_{\mathrm{d}} < 3 \times 10^{-3}$ the relative error of this numerical approximation is less than 2×10^{-6}. The following approximation is applicable in the opposite regime, $\overline{R}_{\mathrm{d}} \gg 1$:

$$\overline{U}(\overline{R}_{\mathrm{d}}) \simeq 1 + 2W_0/\overline{R}_{\mathrm{d}} + 2W_1/\overline{R}_{\mathrm{d}}{}^2 + \frac{W_2}{\pi \overline{R}_{\mathrm{d}}{}^3} + \frac{W_3}{\pi \overline{R}_{\mathrm{d}}{}^4} + \frac{W_4}{\pi \overline{R}_{\mathrm{d}}{}^5} \qquad \text{(C11)}$$

where W_0 is defined in eq B12, $W_1 \approx 0.134\,514$, $W_2 \approx 0.674\,35$, $W_3 \approx 0.314$, and $W_4 \approx 1.81$. The numerical approximation, eq C11, is good within the same error (2×10^{-6}) for $\overline{R}_{\mathrm{d}} > 5$.

References and Notes

(1) Elias, H.-G. The study of association and aggregation via light scattering. In *Light Scattering from Polymer Solutions*; Huglin, M. B., Ed.; Academic Press: London, 1972; Chapter 9.
(2) Hamley, I. W. *The Physics of Block Copolymers*; Oxford University Press: Oxford, UK, 1998.
(3) Israelachvili J. N. *Intermolecular and Surface Forces*; Academic Press: New York, 1985.
(4) Leibler, L.; Orland, H.; Wheeler, J. *J. Chem. Phys.* **1983**, *79*, 3550.
(5) Rubinstein, M.; Colby, R. H. *Polymer Physics*; Oxford University Press: Oxford, UK, 2003.
(6) Zhang, L. F.; Eisenberg, A. *Science* **1995**, *268*, 1728.
(7) Zhulina, E. B.; Adam, M; LaRue, I.; Sheiko, S. S.; Rubinstein, M. *Macromolecules* **2005**, *38*, 5330.
(8) Nyrkova, I. A.; Semenov, A. N. *Eur. Phys. J. E* **2005**, *17*, 327.
(9) Aggeli, A.; Nyrkova, I. A.; Bell, M.; Harding, R.; Carrick, L.; McLeish, T. C. B.; Semenov, A. N.; Boden, N. *Proc. Natl. Acad. Sci. U.S.A.* **2001**, *98*, 11857.
(10) Aggeli, A.; Boden, N.; Carrick, L. M.; McLeish, T. C. B.; Nyrkova, I. A.; Semenov, A. N. Self-Assembling Peptide Gels. In *Molecular Gels: Materials with Self-Assembled Fibrillar Networks*; Weiss, R. G., Terech, P., Eds.; Springer: Berlin, 2006; pp 99−130.
(11) Fischer, E. W. *Physica A* **1993**, *201*, 183.
(12) Kanaya, T.; Patkowski, A.; Fischer, E. W.; Seils, J.; Glaser, H.; Kaji, K. *Acta Polym.* **1994**, *45*, 137.
(13) Kanaya, T.; Patkowski, A.; Fischer, E. W.; Seils, J.; Glaser, H.; Kaji, K. *Macromolecules* **1995**, *28*, 7831.
(14) Brown, W.; Stepanek, P. *J. Polym. Sci., Part B* **1997**, *35*, 1013.
(15) Meier, G.; Vlassopoulos, D.; Fytas, G. *Europhys. Lett.* **1995**, *30*, 325.
(16) Walkenhorst, R.; Selser, J. C.; Piet, G. *J. Chem. Phys.* **1998**, *109*, 11043.
(17) Anastasiadis, S. H.; et al. *Phys. Rev. Lett.* **1993**, *70*, 2415.
(18) Jian, T.; et al. *Macromolecules* **1994**, *27*, 4762.
(19) Stepanek, P.; Lodge, T. P. *Macromolecules* **1996**, *29*, 1244.
(20) Collin, D.; Martinoty, P. *Physica A* **2003**, *320*, 235.
(21) Mendil, H.; Baroni, P.; Noirez, L. *Eur. Phys. J. E* **2006**, *19*, 77.
(22) Collin, D.; Martinoty, P. *Eur. Phys. J. E* **2006**, *19*, 87.
(23) Mendil, H.; Baroni, P.; Noirez, L. *Eur. Phys. J. E* **2006**, *19*, 99.
(24) McKenna, G. B. *Eur. Phys. J. E* **2006**, *19*, 101.
(25) Collin, D.; Martinoty, P. *Eur. Phys. J. E* **2006**, *19*, 109.
(26) Vlassopoulos, D. *Eur. Phys. J. E* **2006**, *19*, 113.
(27) Chushkin, Y.; Caronna, C.; Madsen, A. *Eur. Phys. Lett.* **2008**, *83*, 36001.
(28) Adam, G.; Gibbs, J. H. *J. Chem. Phys.* **1965**, *43*, 139.
(29) Bendler, J. T.; Shlesinger, M. F. *J. Phys. Chem.* **1992**, *96*, 3970.
(30) Sillescu, H. *J. Non-Cryst. Solids* **1999**, *243*, 81.
(31) de Gennes, P. G. *C. R. Phys.* **2002**, *3*, 1263.
(32) Nyrkova, I. A.; Semenov, A. N. *Macromol. Theory Simul.* **2005**, *14*, 569.
(33) Natta, G. *J. Polym. Sci.* **1955**, *16*, 143.
(34) Sinn, H.; Kaminsky, W.; Vollmer, H.-J.; Woldt, R. *Angew. Chem., Int. Ed.* **1980**, *19*, 390.
(35) Williams, A. D.; Flory, P. J. *J. Am. Chem. Soc.* **1969**, *91*, 3111.
(36) Yoon, D. Y.; Sundararajan, P. R.; Flory, P. J. *Macromolecules* **1975**, *8*, 776.
(37) Bovey, F. A.; Hood, F. P.; Anderson, E. W.; Snyder, L. C. *J. Chem. Phys.* **1965**, *42*, 3900.
(38) Johnson, L. F.; Heatley, F.; Bovey, F. A. *Macromolecules* **1970**, *3*, 175.
(39) Bliznyuk, V. N.; Assender, H. E.; Briggs, G. A. D. *Macromolecules* **2002**, *35*, 6613.

(40) Sperling, L. H. *Introduction to Physical Polymer Science*; John Wiley & Sons: New York, 1992.
(41) Fox, T.; Flory, P. *J. Polym. Sci.* **1954**, *14*, 315.
(42) Eisenberg, A. *Macromolecules* **1970**, *3*, 147.
(43) Eisenberg, A.; Hird, B.; Moore, R. B. *Macromolecules* **1990**, *23*, 4098.
(44) Moore, R. B.; Bittencourt, D.; Gauthier, M.; Williams, C. E.; Eisenberg, A. *Macromolecules* **1991**, *24*, 1376.
(45) Shakhnovich, E. I.; Gutin, A. M. *J. Phys.* (*Paris*) **1989**, *50*, 1843.
(46) Gutin, A. M.; Sfatos, C. D.; Shakhnovich, E. I. *J. Phys. A* **1994**, *27*, 7957.
(47) Sfatos, C. D.; Gutin, A. M.; Shakhnovich, E. I. *J. Phys. A* **1994**, *27*, L411.
(48) Sfatos, C. D.; Gutin, A. M.; Shakhnovich, E. I. *Phys. Rev. E* **1995**, *51*, 4727.
(49) Angerman, H.; Ten Brinke, G.; Erukhimovich, I. *Macromolecules* **1996**, *29*, 3255.
(50) Semenov, A. N. *J. Phys. II Fr.* **1997**, *7*, 1489.
(51) Semenov, A. N.; Likhtman, A. E. *Macromolecules* **1998**, *31*, 9058.
(52) Semenov, A. N. *Eur. Phys. J. B* **1999**, *10*, 497.
(53) Subbotin, A. V.; Semenov, A. N. *Eur. Phys. J. E* **2002**, *7*, 49.
(54) Semenov, A. N. *Phys. Rev. E* **2006**, *73*, Art. No. 041803.
(55) Semenov, A. N. *Macromolecules* **2004**, *37*, 226.
(56) Semenov, A. N. *Phys. Rev. E* **1999**, *60*, 3076.
(57) Semenov, A. N. *Europhys. Lett.* **2006**, *76*, 1116.
(58) De Gennes, P. G. *J. Phys.* (*Paris*) **1976**, *37*, 1443.
(59) De Gennes, P. G. *Macromolecules* **1980**, *13*, 1069.
(60) Alexander, S. *J. Phys.* (*Paris*) **1977**, *38*, 983.
(61) Semenov, A. N. *Sov. Phys. JETP* **1985**, *61*, 733.
(62) Milner, S. T. *Science* **1991**, *251*, 905.
(63) Witten, T. A.; Leibler, L.; Pincus, P. *Macromolecules* **1990**, *23*, 824.
(64) Likhtman, A. E.; Semenov, A. N. *Europhys. Lett.* **2000**, *51*, 307.
(65) Grosberg, A.; Khokhlov, A. *Statistical Physics of Macromolecules*; American Institute of Physics: New York, 1994.
(66) Ishihara, N.; et al. *Macromolecules* **1986**, *19*, 2464.
(67) Grassi, A.; et al. *Gazz. Chim. Ital.* **1987**, *117*, 249.
(68) Brandrup, J.; Immergut, E. H.; Grulke, E. A.; Abe, A.; Bloch, D. R. *Polymer Handbook*; Wiley-InterScience: New York, 1999.
(69) Al-Hussein, M.; Strobl, G. *Macromolecules* **2002**, *35*, 1672.
(70) Strobl, G. *Eur. Phys. J. E* **2005**, *18*, 295.
(71) Note that M stands for M_w here and below.
(72) Xu, H.; Ince, B. S.; Cebe, P. *J. Polym. Sci., Part B* **2003**, *41*, 3026.
(73) Diaz, N.; Simon, F. X.; Schmutz, M.; Rawiso, M.; Decher, G.; Jestin, J.; Mesini, P. J. *Angew. Chem., Int. Ed.* **2005**, *44*, 3260–4.
(74) Nyrkova, I. A.; Semenov, A. N., manuscript in preparation.
(75) Semenov, A. N.; Nyrkova, I. A.; Khokhlov, A. R. In *Ionomers: Characterization, Theory and Applications*; Schlick, S., Ed.; CRC Press: Boca Raton, FL, 1996; pp 251−279.
(76) Semenov, A. N.; Nyrkova, I. A.; Khokhlov, A. R. *Macromolecules* **1995**, *28*, 7491−7500.
(77) Raphael, E.; de Gennes, P.-G. *Physica A* **1991**, *177*, 294.
(78) Hilger, C.; Drager, M.; Stadler, R. *Macromolecules* **1992**, *25*, 2498.
(79) Hilger, C.; Stadler, R. *Macromolecules* **1992**, *25*, 6670.
(80) Bredas, J . L.; Chance, R. R.; Silbey, R. *Macromolecules* **1988**, *21*, 1633.
(81) The triangular *R*3*c* symmetry characteristic, for example, for the standard form of crystal structure of iPS involving alternating left-handed and right-handed 3_1 helices[82] is also compatible with the hexagonal shape of the core.
(82) Natta, G.; Corradini, P.; Bassi, I. W. *Nuovo Cimento* **1960**, *Suppl. 15* (10), 68.
(83) Of course, we always assume that the chains are in the polymer brush regime, i.e., that they are strongly stretched in the corona (at least near the core), which is true if $\tilde{N} \gg 1$ (more precisely, $\tilde{N} > b^2/\tilde{L}_1^2$).
(84) A rather similar, but distinct, approximation was introduced in ref 87.
(85) The first model (a) cannot be accepted since the rather long atactic "tails" forming amorphous shells around the crystal simply do not have enough space to be accommodated, even if the tails are completely stretched away from the crystal core (are in all-trans conformation). Hence, either the shell must be significantly compressed (by around 10% of volume) or the tails must be significantly overstretched beyond their length in the straight trans state. Since the amorphous melt is nearly incompressible, and a trans chain is nearly inextensible, both processes cost a high energy, $\sim k_BT$ per monomer unit, i.e., many k_BT per chain. By contrast, the entropic free energy gain due to arbitrary location of the stereoregular sequence along the chain is $\sim k_BT$ per chain, so it is dominated by the overcrowding effect. As a matter of fact, it is likely that the optimal micelle structure involves a mixture of chains with one and two long tails; the latter component is expected to be in minority. This structure results in a somewhat more stable micellar state, hence a wider region of micelles and their larger volume fraction. However, an analysis shows that the free energy gain due to the mixed structure is small ($< k_BT$ per long chain); i.e., the thermodynamic effect of mixing is weak. For this reason (and for simplicity) the more complicated mixed micellar structure is not considered below.
(86) Note that it is the absolute temperatures (in K) that enter all the equations here and below. Yet, in all the numerical examples (including the figures) the temperatures are expressed in °C.
(87) Williams, D. R. M.; Fredrickson, G. H. *Macromolecules* **1992**, *25*, 3561.
(88) Heckmeier, M.; Mix, M.; Strobl, G. *Macromolecules* **1997**, *30*, 4454.
(89) Brown, W.; Nicolai, T. *Macromolecules* **1994**, *27*, 2470.
(90) Nyden, M.; Söderman, O. *Macromolecules* **2000**, *33*, 1473.
(91) This idea will be discussed in more detail separately.
(92) Daniel, C.; Menelle, A.; Brulet, A.; Guenet, J.-M. *Polymer* **1997**, *38*, 4193.
(93) Note that the "ultraslow" cluster relaxation mode can be visible also in the intensity correlation function of the VH scattering component (see Figure 2 in ref 12).
(94) Vasilevskaya, V. V.; Kalatur, P. G.; Khokhlov, A. R. *Macromolecules* **2003**, *36*, 10103.
(95) Maresov, E. A.; Semenov, A. N. *Macromolecules* **2008**, *41*, 9439.
(96) Walter, R.; Selser, J. C.; Smith, M.; Bogoslovov, R.; Piet, G. *J. Chem. Phys.* **2002**, *117*, 427.
(97) Kivelson, D.; Tarjus, G. *J. Non-Cryst. Solids* **2002**, *307*, 630.
(98) Silberberg, A. *J. Colloid Interface Sci.* **1982**, *90*, 86.
(99) Eisenriegler, E. *Polymers near Interfaces*; World Scientific Publishing: Singapore, 1993.
(100) Keller, A. *Philos. Mag.* **1957**, *2*, 1171.
(101) Wunderlich, B. *Macromolecular Physics*; Academic Press: New York, 1973; Vol. *1*.